

**Lightning NO_x Production per Flash based on OMI NO₂
Observations for the Gulf of Mexico**

Allison M. Ring

**Department of Atmospheric and Oceanic Science
University of Maryland, College Park**

Advisors: Dr. Kenneth E. Pickering & Dr. Dale J. Allen

In partial requirement for the Degree of Masters of Science

Submitted on: May 23rd, 2014

Abstract

In this study we evaluate nitric oxide and nitrogen dioxide (together known as NO_x) production from convective storms in the Gulf of Mexico region for August 2008 and July 2011. To do this, we use data from the World Wide Lightning Location Network (WWLLN), a ground based lightning detection network along with data from the Ozone Monitoring Instrument (OMI) aboard NASA's Aura satellite. A processing algorithm is used to remove the stratospheric contribution and includes an air mass factor appropriate for the profile of lightning NO_x .

WWLLN flashes are totaled over 6-hour and 3-hour time periods prior to OMI overpass, and various flash thresholds are applied to isolate convective storms. Analyses are also completed using pixels with various cloud radiative fraction (CRF) criteria. The method discussed in this paper is most appropriate over regions with minimal anthropogenic sources and regions of active convection.

We conclude that the best estimates of lightning NO_x over active convection in the Gulf of Mexico come from analyses using $\text{CRF} > 70\%$, flashes from the 3 hours prior to OMI overpass, and a flash threshold of 500 flashes. For both August 2008 and July 2011, we obtained approximately 330 moles per flash over this region. These values are consistent with literature estimates.

Table of Contents

Abstract

Table of Contents

1. Introduction

2. Background

2.1 LNO_x and Upper Troposphere Ozone Production

2.2 NO Production from Lightning

3. Data and Methods

3.1 Ozone Monitoring Instrument

3.2 World Wide Lightning Location Network

3.3 Global Modeling Initiative – Chemical Transport Model

3.4 Algorithm

4. Results

4.1 Initial Approach

4.1.1 August 2008

4.1.2 July 2011

4.1.3 Conclusions

4.2 Active Convection Analysis– June 11th DC3 Case

4.3 Analysis with Active Convection over the Gulf of Mexico

4.3.1 August 2008

4.3.2 July 2011

5. Discussion and Conclusions

6. References

1. Introduction

Global emissions of nitric oxide (NO) and nitrogen dioxide (NO₂), known together as NO_x, are dominated by anthropogenic sources such as commercial and residential fossil fuel combustion, electricity generation, and fossil fuel extraction. In the lower troposphere, air quality effects of NO_x emissions are most notable through their reactive contribution to tropospheric ozone (O₃) formation. Exposure to high O₃ mixing ratios can contribute to negative health consequences including lung related illnesses such as asthma, especially for people in high-risk age groups.

In the lower troposphere, the dominant form of NO_x is NO₂ because NO reaction with ozone occurs at a faster rate than NO₂ conversion back to NO through photolysis. NO₂ then reacts with the hydroxyl radical (OH), the primary oxidizing species in the atmosphere, to produce nitric acid (HNO₃), which is then wet or dry deposited (*Seinfeld and Pandis, 2006; Schumann and Huntrieser, 2007*). This results in a NO_x lifetime of approximately 1 to 2 days in the lower troposphere (*Seinfeld and Pandis, 2006*).

While approximate source strengths for anthropogenically produced NO_x are known (*Zhang et al., 2003; Schumann and Huntrieser, 2007*), considerable uncertainty exists for naturally produced NO_x. Lightning is the largest natural source of NO_x, produced from splitting N₂ and O₂ diatomic molecules as a result of the extreme heat from lightning, forming NO, a process commonly referred to as the Zel'dovich Mechanism (*Zel'dovich et al. 1947*). This occurs primarily in the middle and upper troposphere due to lightning activity in convectively active regions, and contributes approximately 70% of the total NO_x concentration in the subtropical and tropical free troposphere (*Tie et al., 2002; Schumann and Huntrieser, 2007*).

In the upper troposphere, NO_x has a lifetime on the order of a week (*Jaeglé et al., 1998, Martin et al., 2007*), because temperatures are colder and reaction rates are slowed (*Seinfeld and Pandis, 2006*). At this altitude, NO_x can experience long-range transport (*Gallardo and Cooray, 1996*), and O_3 production is more efficient in the upper troposphere than in the lower troposphere (*Pickering et al., 1996; DeCaria et al., 2005; Ott et al., 2007*). Accurate measurement of lightning-produced NO_x from space is difficult because anthropogenic sources are prolific and dominate total column satellite measurements. Contributing to the lightning NO_x (LNO_x) production uncertainty, cloud-to-ground (CG) and intracloud (IC) lightning strokes may produce different amounts of NO_x due to differences in their energy per stroke and path length (*Gallardo and Cooray, 1996; Price et al., 1997*). In a changing climate, it is critical to develop a stronger understanding of the LNO_x contribution to middle and upper tropospheric O_3 production because O_3 is considered the third most important greenhouse gas (*IPCC 2013*). It is a secondary pollutant; produced in the atmosphere via chemical reactions of precursors such as NO_x . The ability of climate models to capture the contributions of LNO_x to O_3 production is needed for accurate climate prediction.

In this study, we focus on the Gulf of Mexico region, specifically between latitudes 24°N and 30°N and longitudes 74°W and 100°W . This region is well covered by several ground-based lightning detection networks, and experiences minimal to moderate anthropogenic influence; an important consideration for choosing a site because approximately 30% of all NO_x detected in anvils above populated areas derives from production within the planetary boundary layer (PBL) (*Huntrieser et al., 2002*). To estimate the source strength of LNO_x , the flash rate and LNO_x production per flash are required. To determine the flash rate, we use

the World Wide Lightning Location Network (WWLLN), a ground-based detection network out of the University of Washington, and two satellite based instruments: the Optical Transient Detector (OTD) in use between 1995-2000 (*Christian et al., 2003; Boccippio et al., 2000*) and the Lightning Imaging Sensor (LIS) operating from 1997 to present (*Christian et al., 1999, 2003; Boccippio et al., 2002; Mach et al., 2007*). The data from these two instruments are combined to create the lightning climatology (*Cecil et al., 2012*) used in this study.

Due to the combination of ground-based and satellite-based lightning detection data, the mean regionally-averaged lightning flash rate is relatively well understood. Therefore, one reason for the difficulty in representing LNO_x emissions in climate models is the uncertainty surrounding the moles of LNO_x produced per flash (see Table 1, Section 2.2). Other reasons for the LNO_x emissions uncertainty include biases in convective precipitation, and in the relationship between convective parameters and flash rates (*Pickering et al., 1998; Allen and Pickering, 2002*). In this study, we will focus on estimation of the moles of LNO_x production per flash in an effort to reduce the uncertainty in the LNO_x emissions. To do this, we use a processing algorithm to extract the column LNO_x from the OMI data. In this algorithm, we use modeled LNO and LNO₂ profiles to convert the LNO₂ estimated from OMI to LNO_x. We then examine the flashes coincident with the OMI LNO_x over various time intervals prior to OMI overpass to generate an estimated moles of LNO_x produced per flash for the region. Expansion of the principles learned through this study to a global analysis is ongoing.

2. Background

2.1 LNO_x and Upper Troposphere Ozone Production

Ozone is important to atmospheric oxidation reactions and atmospheric radiative forcing (*Huntrieser et al., 2011; IPCC, 2013*). Lightning contributes significantly to the upper tropospheric concentration of NO, an important O₃ precursor. Therefore, a better understanding of the LNO_x source strength in tropical regions and mid-latitude summer months where lightning flash rates are high is required.

An estimated 60-90% of upper tropospheric NO_x concentrations and 15-35% of upper tropospheric O₃ concentrations over the United States during June, July and August come from lightning NO (*Allen et al., 2010*). The contribution varies regionally; however, the scientific community is in agreement that upper tropospheric NO_x concentrations predominantly derive from lightning flashes, and that a significant portion of upper tropospheric O₃ production is attributable to LNO_x production.

Other important precursors to tropospheric O₃ are the hydroxyl radical (OH) and the hydroperoxyl radical (HO₂) known together as HO_x. In the upper troposphere, HO_x is enhanced due to the convective transport of HO_x precursors such as peroxides and formaldehyde. A maximum in HO_x concentrations contributes to a peak in O₃ production on a short time scale (~4 hours) over and immediately downwind of active convection (*DeCaria et al., 2005*). LNO_x has been shown to enhance O₃ production several days downwind of active convection, in part due to the longer lifetime of NO_x in the upper troposphere (*Pickering et al., 1993; 1996*). Clear skies downwind from active convection result in strong photolysis of NO₂, enhancing O₃ production especially between 500-300 hPa (*Labrador et al., 2005*). *DeCaria et al. (2005)*, found a maximum O₃ increase of 10-13

ppb downwind of active convection at 10.5 km. *Hauglustaine et al. (2001)* found similar O₃ enhancements of 10-20ppb using global model simulations with and without LNO_x contributions. Analogous enhancements in O₃ concentrations were found for both the NH and SH mid-latitude regions during the respective summer seasons confirming that the impact of LNO_x on upper tropospheric O₃ formation is a global phenomenon.

2.2 NO Production from Lightning

To understand the global LNO_x and O₃ upper tropospheric budget, an estimation of NO production from lightning is necessary. Current literature estimates of NO production per flash vary considerably for lightning events in tropical and mid-latitude regimes (see Table 1). These estimates have been generated from theoretical analyses, model studies, and in situ aircraft measurements during aircraft campaigns. NASA's Global Modeling Initiative (GMI) chemical transport model assumes a mid-latitude lightning flash NO mean production value of 500 moles, and a tropical lightning flash NO mean production value of 250 moles (*Allen et al., 2010*). These models generally do not distinguish between IC and CG flash production rates because further study is necessary to clarify if there is a significant difference between them.

As seen in Table 1, estimates range from 32 to 1100 moles of NO per flash. Considering the large uncertainty in the moles of NO production per flash estimates, model assumptions may be inaccurate, thus preventing accurate upper tropospheric chemistry modeling. The values from Table 1 are from studies of storm events, which are then extrapolated to global estimations. The table suggests that geographic location, the mid-latitudes (blue) vs. the tropics (red), of individual storms affects the LNO_x production per flash.

Table 1: Compilation of literature estimates of lightning generated NO moles per flash.

Method	Moles NO/flash (Notes)	Reference
Theoretical	1100 (CG), 110 (IC)	Price et al., 1997
Laboratory	~103	Wang et al., 1998
LMA/Theoretical	484 (CG), 35 (IC)	Koshak et al., 2014
Aircraft data, cloud model	345-460 (STERAO-A)	DeCaria, et al., 2005
Aircraft data, cloud model	360 (STERAO-A, EULINOX)	Ott et al., 2007; 2010
Aircraft data, cloud model	590-700 (CRYSTAL-FACE)	Ott et al., 2010
	500 (Mean mid-latitude)	Ott et al., 2010
Aircraft data, cloud model	500 – 600 (SCOUT-O3/ACTIVE)	Cummings et al., 2013
Aircraft data	70-210 (TROCCINOX)	Huntrieser et al. 2008
Aircraft data	121 – 385 (SCOUT-O3/ACTIVE)	Huntrieser et al., 2009
Aircraft data	70 – 179 (AMMA)	Huntrieser et al., 2011
Satellite (GOME)	32-240 (Sub-Tropical)	Beirle et al., 2006
Satellite (SCIAMACHY)	33 – 50 (global, mostly marine)	Beirle et al., 2010
Satellite (OMI)	87-246 (TC4 – tropical marine)	Bucsela et al., 2010
	174 (TC4 mean)	Bucsela et al., 2010

Modeling studies have examined the significance of this variation in different latitudinal regimes (*Ott et al., 2010*). Laboratory and theoretical estimates support significant difference between the IC and CG flash production of NO (*Price et al., 1997; Koshak et al., 2014*), while modeling based studies constrained by anvil aircraft observations find a much smaller difference between the source strengths of IC and CG flashes (*DeCaria et al., 2005; Ott et al., 2007, 2010; Huntrieser et al., 2011; Cummings et al., 2013*).

With the significant variation in moles of NO per flash values shown in Table 1, a comprehensive study that can be expanded globally is necessary. In this study we use a satellite-based analysis to estimate the NO production per flash. This approach will allow us to examine tropical vs. mid-latitude regional variations in NO production per flash. It will also contribute to determining if the current estimates of 500 moles of NO per flash for mid-latitude storms and 250 moles of NO per flash for tropical storms, used in the GMI global model are accurate.

3. Data and Methods

3.1 Ozone Monitoring Instrument

The Ozone Monitoring Instrument (OMI) is aboard the Aura spacecraft, a member of NASA's A-train sun-synchronous polar orbiting satellite group. OMI detects a variety of molecules and aerosol characteristics, and passes over the equator at 13:30 LT. It measures a 2,600 km swath, with a binned ground pixel size at nadir of 13 x 24 km, increasing to a ground pixel size of about 13 x 150 km at the outer edges of the swath (Levelt *et al.*, 2006a; Levelt *et al.*, 2006b), as shown in Figure 1.

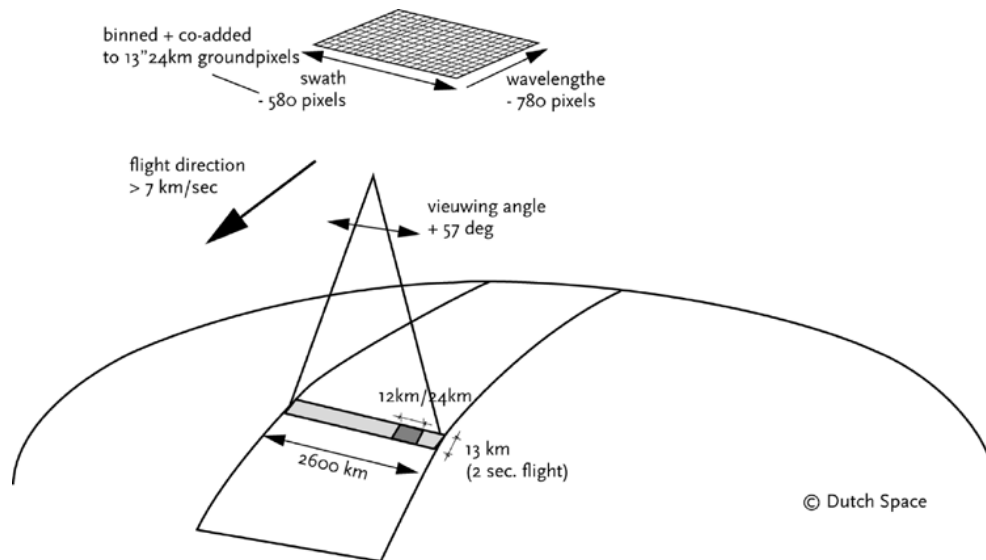


Figure 1: A simple depiction of the OMI measurement principle.
Image source: Levelt *et al.*, 2006a

OMI uses a two dimensional detector which allows for simultaneous retrievals across the field of view. It measures in the UV and visible range, between 270 and 500 nm, with the NO₂ signal derived from the visible range between 425 and 450 nm (Levelt *et al.*, 2006a; Levelt *et al.*, 2006b). We use level 2 processed data, generated from the Differential Optical Absorption Spectroscopy (DOAS) technique algorithm, developed by the Royal Dutch Meteorological Institute (KNMI), which yields a total slant column (Levelt *et al.*, 2006b; Platt

and Stutz, 2006) of NO₂. The standard processing of level 2 data at NASA Goddard was significantly improved in Version 2 from the previous Version 1 processing algorithm because it improves cloud property data, the stratosphere-troposphere separation, and the temporal resolution (was annual is now monthly) of a priori NO₂ profiles (Boersma et al., 2011; Bucselo et al., 2013). Due to an orbital “striping” effect (Boersma et al., 2011; Bucselo et al., 2013), the OMI slant columns are re-processed before level 2 products are produced; a thorough discussion of how this is executed is provided in Bucselo et al. (2013). Using the level 2 processed and de-striped NO₂ total slant column, we convert to vertical column LNO_x using the algorithm described in section 3.4.

For this study, we use OMI measured daily NO₂ global columns for the months of August 2008 and July 2011. As of June 2007, a row anomaly in the OMI data has become evident, likely due to a partial obstruction of OMI’s aperture (Boersma et al., 2011; Bucselo et al., 2013). During August 2008, this minimally affected our data but in July 2011, the row anomaly was significant, requiring a few days of data to be removed from our analysis.

3.2 World Wide Lightning Location Network

The World Wide Lightning Location Network (WWLLN) is a ground-based global network of stations that detect very low frequency (VLF) signals from lightning discharges called sferics within the 3-30 kHz range (Dowden et al., 2002; Lay et al., 2005; Virts et al., 2013). WWLLN began recording reliable lightning data in 2004, and has increased its global coverage from 11 stations to about 70 stations today (Lay et al., 2004; Hutchins et al., 2013). Figure 2 shows the global extent of the WWLLN stations as of December 2012. We use the WWLLN data in conjunction with OMI LNO_x retrievals to estimate the LNO_x production per flash for the Gulf of Mexico.

WWLLN Stations

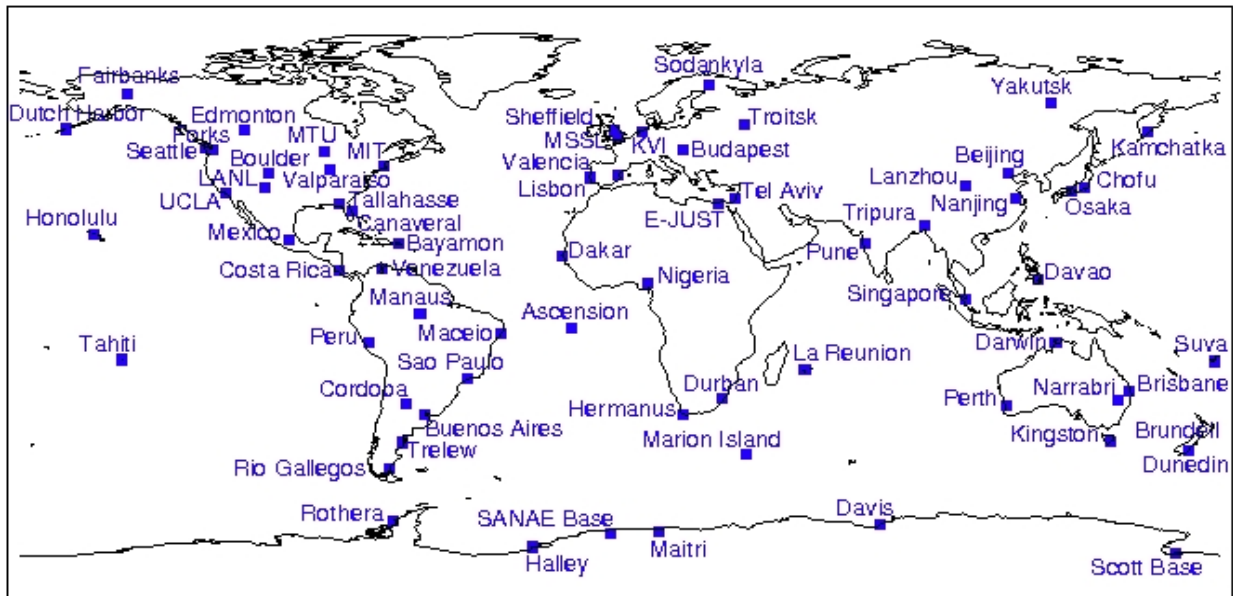


Figure 2: Global distribution of WWLLN stations.

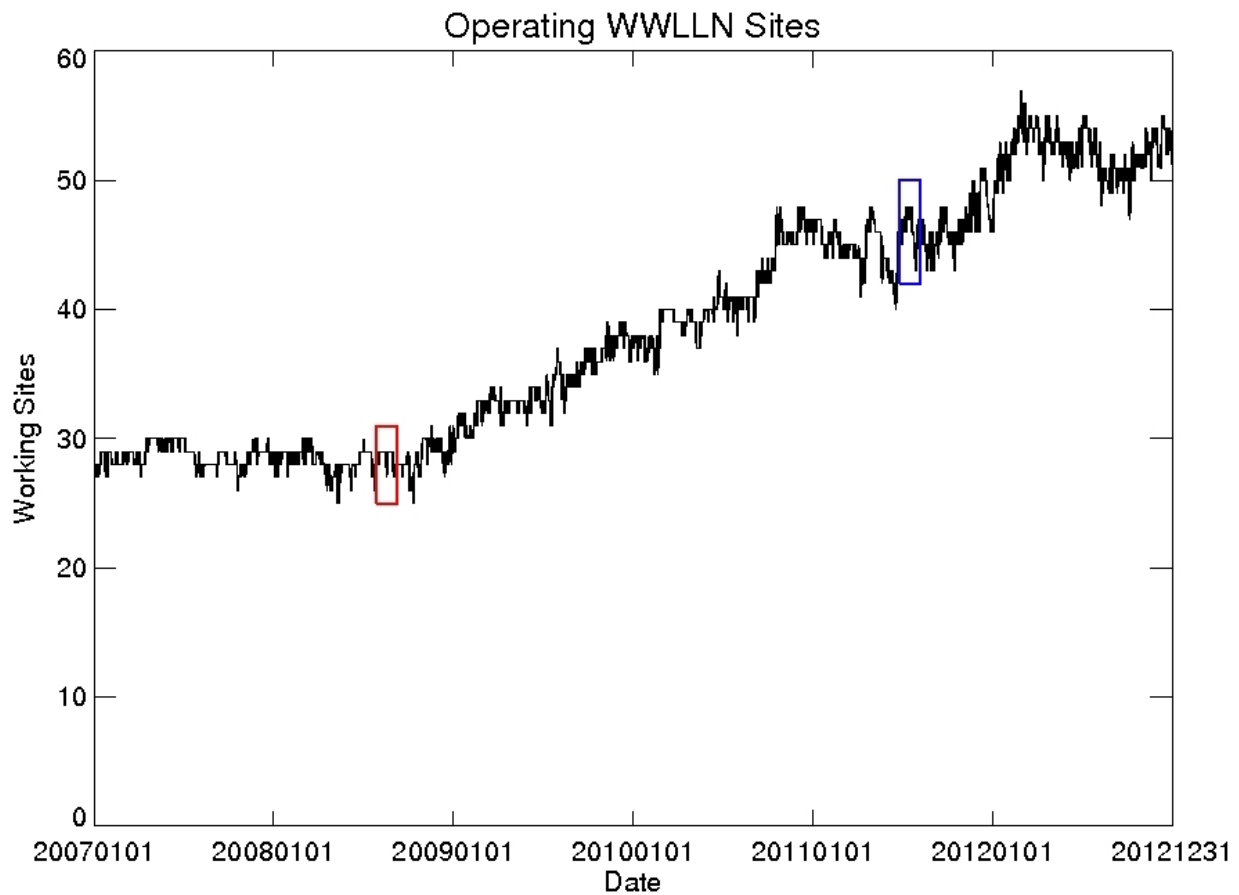


Figure 3: WWLLN stations operating each day between Jan 1, 2007 and Dec 31, 2012. August 2008 (red box) and July 2011 (blue box) are the months used in this study.

Figure 3 shows that the number of working stations increased from approximately 28 in 2007 to approximately 55 in 2012. In August 2008, there are ~28 working stations, and in July 2011, there are ~43 working stations (see boxes in Figure 3). Some stations are in remote locations, and some are in countries troubled by political unrest making their accessibility challenging. This results in intermittency of some stations that can last days or months, negatively affecting the network detection efficiency.

A time of group arrival (TOGA) packet containing the stroke UTC date and time, stroke location, error in microseconds, and the number of stations that received the signal (*Rodger et al., 2004; Rodger et al., 2005*) is recorded. Strong sferic discharges can travel significant distances (up to 10,000 km), especially over water, which is why a global network of less than 100 stations can be reliable for lightning stroke detection (*Lay et al., 2005; Rodger et al., 2009*). In order for a stroke to be counted, a minimum of five WWLLN stations must detect a lightning signal (*Dowden et al., 2002; Rodger et al., 2005*). Due to its detection frequency range (3-30 kHz), WWLLN is most efficient at detecting cloud to ground strokes, but can detect some inter-cloud activity (*Rodger et al., 2009; Rudlosky and Shea, 2013*). For a more detailed description of the WWLLN processing algorithm, please refer to the paper by *Rodger et al. (2004)*.

We use lightning climatology data from OTD/LIS to estimate the detection efficiency of WWLLN strokes with respect to OTD/LIS flashes as a function of time and space. Analysis with ground-based networks are needed for obtaining a continuous record of individual flashes because LIS flies aboard the Tropical Rainfall Measurement Mission (TRMM) satellite between 35°N and 35°S (*Christian et al., 2003; Boccippio et al., 2002*) and samples a particular field of view (600 x 600 km) for approximately 90 seconds (*Christian et al., 1999;*

Cecil et al., 2012) each day. The flash detection efficiency of LIS ranges from 68% at noon to 88% at night (*Christian et al., 1999; Boccippio et al., 2002*). Due to its space-based platform, LIS cannot distinguish between IC and CG flashes (*Christian et al., 1999*).

To begin, the WWLLN data are gridded on a 2° latitude x 2.5° longitude grid (GMI grid), and a 1° x 1° latitude/longitude grid. The next step is to determine the detection efficiency of WWLLN strokes with respect to OTD/LIS flashes as a function of grid box and time (month). The WWLLN detection efficiency is simply the reciprocal of the scaling factor by which the gridded WWLLN flash rates must be multiplied in order to ensure the annual average WWLLN flash rate matches the OTD/LIS flash rate for that time period. In order to minimize the noise in the resulting detection efficiencies, the gridded WWLLN flash rates are smoothed temporally and spatially before the scaling factors are determined. The smoothers include a running 31-day average, a 3-hour average, and a 3-pt north-south and east-west boxcar smoother. Annual scaling factors for each grid box are then determined by comparing smoothed WWLLN stroke rates and OTD/LIS flash rates for the 61 consecutive 12-month periods between January 2005 and December 2012. Monthly scaling factors are then obtained by averaging the annual scaling factors from the twelve 12-month time periods that contain the month of interest. These 12-month periods include 11 months before and after the month of interest. Therefore, the final monthly scaling factor for each grid box is a weighted average with the month of interest having a weighting of 12. The weighting factor for other months is equal to 12 minus the number of months the other month is removed from the month of interest. The monthly scaling factors are applied to the raw WWLLN gridded data to create OTD/LIS detection-efficiency adjusted WWLLN flash rates. Finally, an optional diel adjustment can be applied to the detection-

efficiency adjusted WWLLN flash rates. This step ensures that the diel variation in detection-efficiency adjusted WWLLN flash rates matches the diel variation in version 2.3 of the OTD/LIS climatology (see also *Allen et al., 2014*).

3.3 Global Modeling Initiative – Chemical Transport Model

To model the mean monthly NO and NO₂ profiles, we used output from the NASA Global Modeling Initiative (GMI) chemical transport model simulations that were performed with and without lightning. These monthly mean profiles are used in the algorithm to calculate air mass factors, described in section 3.4. GMI is a NASA supported coupled troposphere and stratosphere model (*Duncan et al., 2007, Ziemke et al., 2006*) that includes chemistry and transport, deposition, radiation, and aerosol microphysics (*Duncan et al., 2007*). More specifically, we used GMI HindcastFF simulations which incorporate Aura Harvard ship emissions, and year specific fossil fuel emissions based on EDGAR (Emission Database for Global Atmospheric Research) 2000 data with various regional inventories and GEOS-Chem (Goddard Earth Observing System-Chemical Transport Model) scaling factors applied for other years (*van Donkelaar et al., 2008*). HindcastFF simulations also use year specific GFEDv3 (Global Fire Emissions Database v.3) biomass burning emissions (*van der Werf et al., 2010*) with diurnal variation and emission factors from GEOS-Chem, Asian fossil fuel emissions from *Streets et al.* inventories for 2006 (*Zhang et al., 2009*) scaled to other years using GEOS-Chem scaling factors, and biofuels based on *Yevich and Logan (2003)* but overwritten with data from EPA/NEI99 over the United States.

The GMI model is driven by GEOS-5 meteorological fields at 2° latitude x 2.5° longitude spatial resolution, and a vertical resolution of 72 pressure levels (*Rienecker et al., 2008; Bucseila et al., 2013*). Simulations were executed from June 2006 through December 2012

to provide ample spin-up time for our August 2008 and July 2011 analysis months. To examine the lightning signature from the GMI model, we ran two simulations: one with lightning, and one without lightning. We extracted monthly NO and NO₂ profiles coincident with the OMI overpass time of 13:30 LT. Taking the difference of the vertical profiles between the two simulations yields the modeled LNO_x and LNO₂ vertical profiles, used in the algorithm discussed in section 3.4.

3.4 Algorithm

The full algorithm used to generate the vertical column LNO_x is given by:

$$\Omega_{\text{LNO}_x} = \frac{\Omega_{\text{total}}^{\text{slant}} - \Omega_{\text{strat}}^{\text{OMI}} \times \text{AMF}_{\text{strat}} - \Omega_{\text{BG}}^{\text{OMI}} \times \text{AMF}_{\text{trop}}}{\text{AMF}_{\text{LNO}_x}}$$

where $\Omega_{\text{total}}^{\text{slant}}$ is the OMI measured NO₂ total slant column, $\Omega_{\text{strat}}^{\text{OMI}}$ is the stratospheric NO₂ vertical column, and $\text{AMF}_{\text{strat}}$ is the modeled stratospheric air mass factor used in the standard OMI product (Bucsela et al., 2013). $\Omega_{\text{BG}}^{\text{OMI}}$ is the estimated tropospheric vertical column due to all non-lightning NO₂ sources, treated multiple ways in this analysis as discussed later in section 3.4. AMF_{trop} is the modeled tropospheric air mass factor used in the standard OMI product (Bucsela et al., 2013), and $\text{AMF}_{\text{LNO}_x}$ is the air mass factor used to convert the slant column of LNO₂ to a vertical column of LNO_x. It is derived from radiative transfer modeling and uses the profile of LNO_x/LNO₂ derived from the GMI simulations. For a thorough discussion of the $\text{AMF}_{\text{strat}}$ and AMF_{trop} used in this analysis, please refer to the Bucsela et al. (2013) paper. The calculated column LNO_x is produced for each OMI pixel and the total LNO_x in either 2° x 2.5° GMI grid cells or 1° x 1° grid cells is obtained.

For our initial attempt, we removed the tropospheric background with a 30-day average of the standard tropospheric NO₂ from OMI. We realized this did not accurately remove the non-lightning NO₂ from the OMI data. In many instances, this 30-day average was too large, producing negative LNO_x values. Tropospheric NO₂ from OMI in active convection and cloudy regions includes NO₂ within and above the clouds, but does not include NO₂ below the cloud (*Bierle et al., 2009*). In these environments, the OMI measured column is therefore not the total NO₂ column. Subtraction of the 30-day tropospheric average NO₂ is therefore inappropriate because in these cloudy regions, the lower tropospheric NO₂ contribution is not measured, and therefore, does not need to be subtracted. This explains why subtraction of the 30-day average causes mean LNO_x values to be negative. To examine cloud effects on OMI column NO₂ retrieval, we conducted a cloud radiative fraction threshold sensitivity analysis.

Cloud radiative fraction (CRF) is an OMI observation of the cloud brightness. A CRF of 0% means the OMI pixel is observing a clear sky, straight through to the ground. A CRF of 100% indicates the OMI pixel is observing exceptionally bright (and high) clouds. In especially active convection regions, OMI pixels can observe CRFs greater than 100%. We calculated the lightning-NO column via the processing algorithm four times using pixels with CRFs < 100% (all pixels), < 70%, < 50%, and < 30%.

Even when only clear sky pixels were examined (< 30% CRF), many negative LNO_x values still remained indicating that the tropospheric background removed from the total OMI column was too large. Clearly, analysis of LNO_x downwind of storms will require changes to the method used to determine the tropospheric background term.

Applying CRF thresholds of $< 70\%$, $< 50\%$, or $< 30\%$ removed nearly all grid boxes with active convection. Therefore, we examined LNO_x production over convective storms using thresholds that retained pixels with CRFs greater than 70% and 90%. This eliminated OMI pixels over relatively clear skies and minimal convection, where the majority of the observed column NO_x is due to lower tropospheric sources. For remaining pixels, we assumed all retrieved NO_2 originated with lightning and therefore did not remove a tropospheric background. This assumption is most valid over regions where boundary layer sources of NO_x are small such as rural, remote, and/or marine locations.

4. Results

Our initial algorithm did not distinguish between regions of active convection and regions downwind of convection. It used the same tropospheric background subtraction for both cases. Results of this approach are discussed in Section 4.1, and results for active convection alone are presented in Sections 4.2 and 4.3.

4.1 Initial Approach

In this analysis we used daily OMI NO₂ total slant column data, and subtracted a running 4-day average vertical column of stratospheric NO₂ multiplied by the standard stratospheric AMF. The 4-day average of stratospheric NO₂ includes the two days before and after the day of analysis. We then subtracted the 30-day average tropospheric background vertical column NO₂ multiplied by the tropospheric AMF. In the numerator of the algorithm, the OMI slant column changed daily, the stratospheric component also varied each day, but the 30-day background remained constant for the whole month. The LNO_x AMF denominator was derived from GMI monthly NO and NO₂ profiles, so it too remained constant.

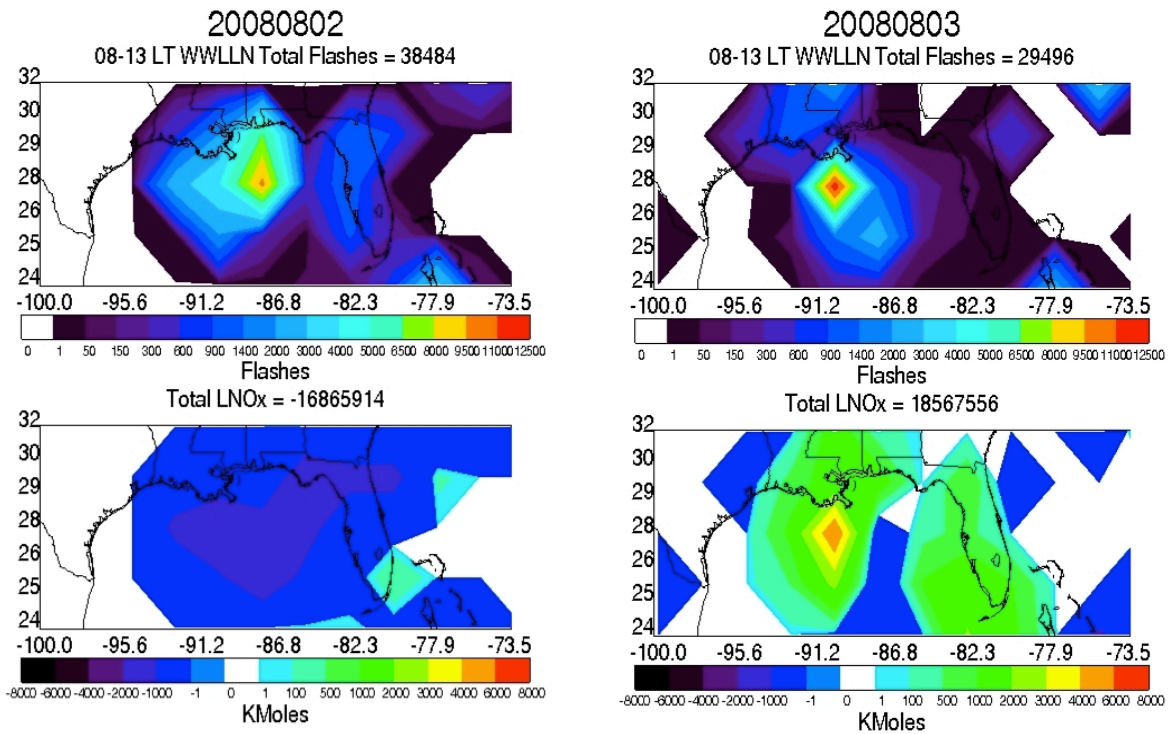
Plots were generated using 2° latitude x 2.5° longitude grid resolution, consistent with the GMI grid. We used all flashes within the 6 hours prior to OMI overpass in the Gulf of Mexico spatial domain. It is assumed that flashes occurring within the 2° x 2.5° grid box 6 hours prior to OMI overpass contribute to the LNO_x portion of the OMI NO₂ column because on average most of the LNO_x produced will likely still remain, and not be transported outside the grid box domain. Daily flash locations constrain the LNO_x; meaning OMI data are only used for grid boxes where lightning flashes occurred in the 6 hours prior to OMI overpass. The 30-day average tropospheric background subtraction is applied as the

average for each grid box, but not all grid boxes are used each day due to the lightning constraint. Analysis for August 2008 and July 2011 using this method were executed.

4.1.1 August 2008

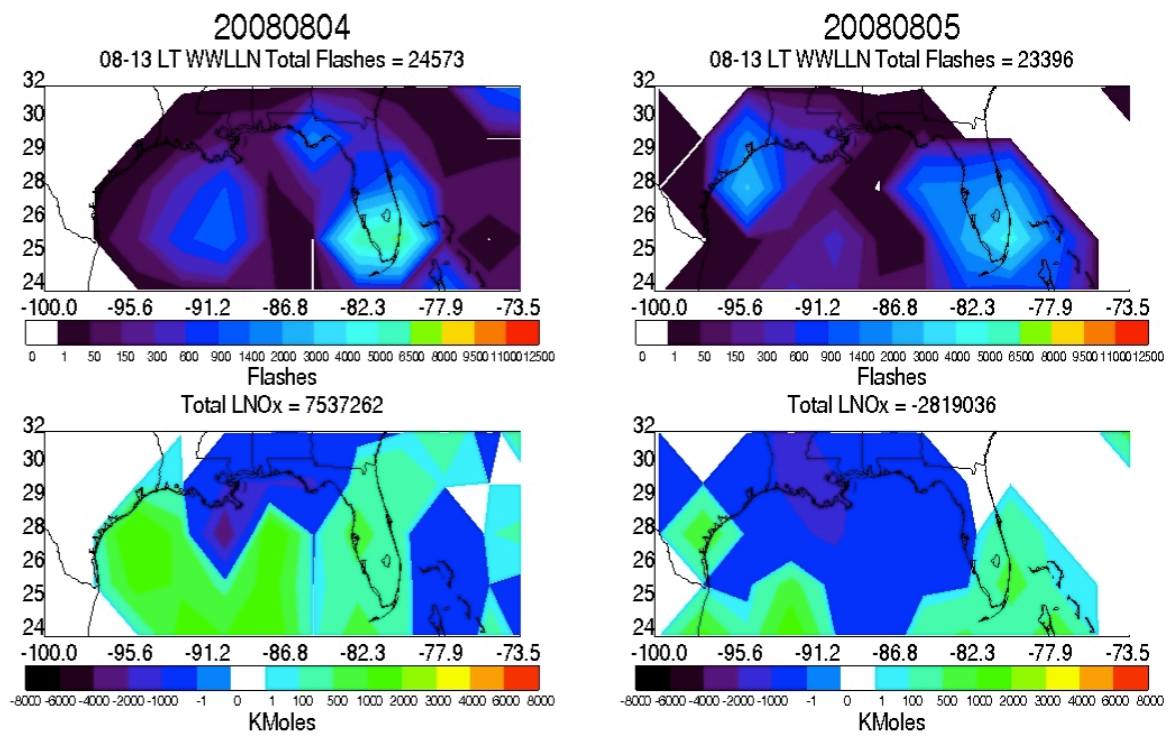
Daily fluctuations in mean LNO_x moles per flash over the Gulf of Mexico region varied from -1000 moles per flash to 700 moles per flash, with the majority as negative values. A +/- 2ppbv limit was applied to LNO_x estimates before moles per flash were calculated because measured and modeled values of NO_x rarely exceed 2ppbv in the upper troposphere for an area as large as the 2° x 2.5° grid box. The -2ppbv limit is used to ensure no positive bias is introduced. Extreme positive and negative LNO_x values were seen before applying this threshold, and are treated in this case as noise. Setting a +/- 2ppbv limit on the generated kmoles of LNO_x limits this noise.

Figure 4 depicts four consecutive days during August 2008. For each day, the total flashes within the 6 hours prior to OMI overpass and the total LNO_x in kmoles are plotted.



a.) Moles/Flash = -438.3 Limit = 2ppb

b.) Moles/Flash = 629.5 Limit = 2ppb



c.) Moles/Flash = 306.7 Limit = 2ppb

d.) Moles/Flash = -120.5 Limit = 2ppb

Figure 4: Total flashes with the sum of the total flashes above the plot, and LNOx in kmoles with the sum of the total LNO_x in moles above the plot for a.) August 2nd, 2008, b.) August 3rd, 2008, c.) August 4th, 2008, d.) August 5th, 2008.

On August 2nd (plot a), a lightning maximum is seen off the tip of Louisiana, but this coincides with negative LNO_x, yielding -438.3 moles per flash. This negative LNO_x indicates the tropospheric background subtraction is too large for this grid box on this day. On August 3rd (plot b) a positive LNO_x signal is seen collocated with a maximum in lightning. This result is more representative of the expected OMI measurement and flash collocation, and yields a value of 629.5 moles per flash. This is slightly high, but well within the literature range. Moving to August 4th (plot c), negative LNO_x is seen in the same location of the LNO_x peak from the previous day. The mean NO production per flash over the Gulf of Mexico region is still positive due to the large positive LNO_x region further south in the Gulf of Mexico, but the lightning plot indicates minimal storm activity in the region. Over south Florida, positive LNO_x is seen with a peak in lightning activity.

On August 5th (plot d), we see very little lightning activity over the water, but the few flashes within the region during the 6 hours prior to OMI overpass are causing negative LNO_x pixels to be used in the moles per flash calculation. Again over south Florida, positive LNO_x is collocated with a peak in lightning. For the whole Gulf of Mexico region, the negative LNO_x results in a -120.5 moles per flash value for the region and may be an artifact from the tropospheric background removal portion of the algorithm (inappropriate background removal in this case).

In this analysis, the lightning flash and LNO_x data are used if a single flash occurred during the 6 hours prior to OMI overpass. From this analysis, we determined this threshold is too low. In analyses discussed later in this paper, we will use higher flash thresholds more indicative of a storm event rather than a few isolated lightning flashes.

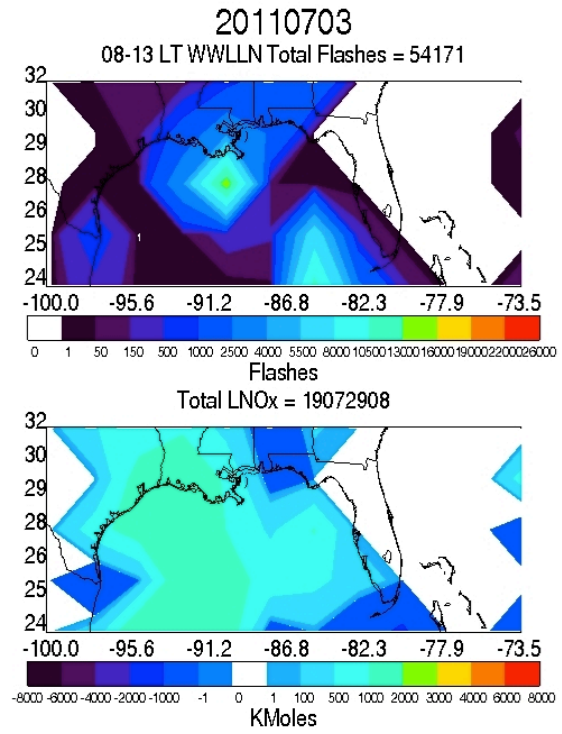
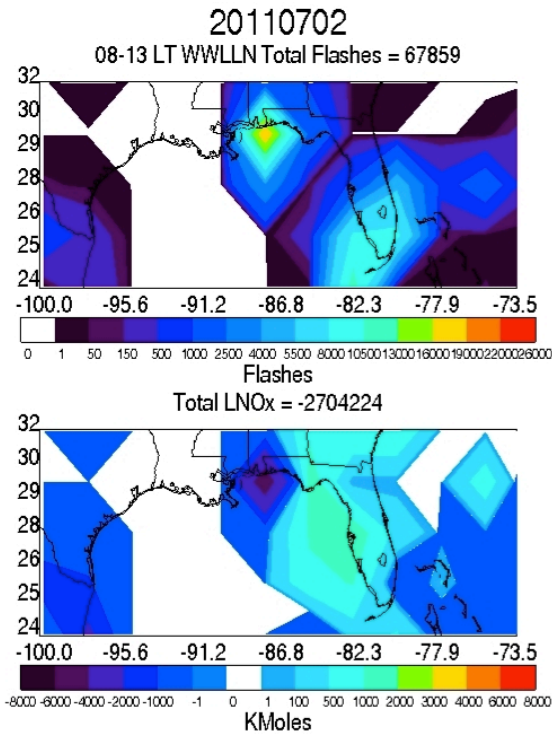
OMI retrievals in August 2008 are minimally affected by the row anomaly. Unfortunately, in August 2008 WWLLN detection efficiency is relatively low as discussed in section 3.2. For this reason, we chose to expand our analysis to include July 2011, a month when WWLLN detection efficiency is better for the Gulf of Mexico, however, the OMI data are more affected by the row anomaly.

4.1.2 July 2011

For July 2011, the increase in WWLLN detection efficiency is coupled with a decrease in OMI data quantity. The row anomaly requires many pixels to be categorized as missing data, necessitating the removal of some pixels from the analysis entirely. As a result of the spotty OMI coverage, storms are sampled less completely. This causes the daily mean moles per flash values for each storm and consequently for the region to vary considerably, ranging from approximately -2500 to 350 moles per flash. This analysis was conducted using the same tropospheric background, stratospheric background, and air mass factor methods as discussed previously for August 2008.

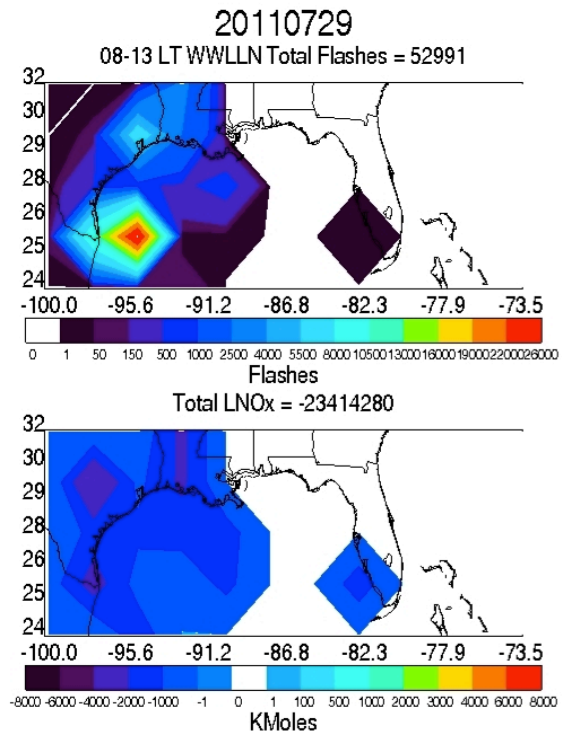
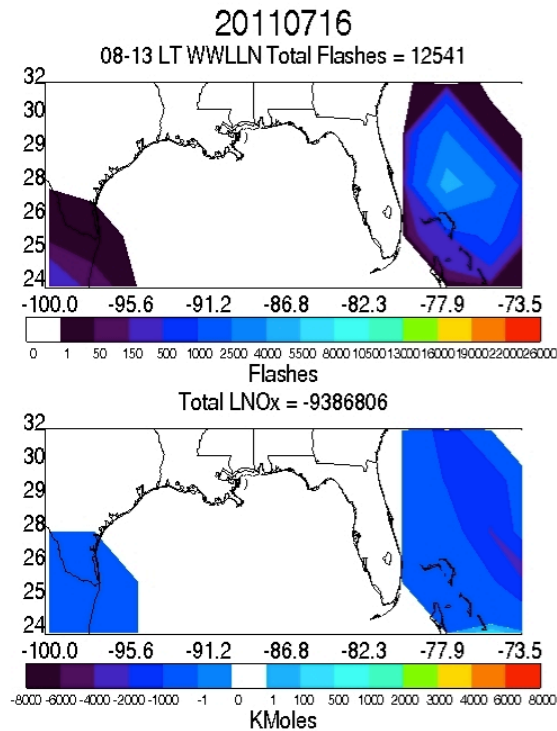
In Figure 5, four days from July 2011 are highlighted. Total flashes in the 6 hours prior to OMI overpass, and kmoles of LNO_x are plotted. Again, on July 2nd (plot a) we see negative LNO_x coincident with a lightning peak. The positive LNO_x off the Gulf coast of Florida elevates the regional moles per flash estimate to -39.9. The source of this positive plume is not clear, as it does not coincide with a peak in lightning activity. On July 3rd (plot b) we see positive LNO_x , along with a minor peak in flashes south of Louisiana, but this lightning does not explain the positive LNO_x large spatial coverage. This day does however yield the largest moles per flash estimate of 352.1 for July 2011. The plot for July 16th (plot c) illustrates the devastating effects of the OMI row anomaly to our analysis. The swath of

missing data is directly over the Gulf region, rendering this day essentially useless. The plotted lightning only corresponds to negative LNO_x values, again raising concern about our treatment of the tropospheric background. Finally, on July 29th (plot d) we again see similar results as plotted on July 2nd and July 16th: peaks in lightning activity collocated with very negative LNO_x . The frequency of this anti-intuitive result is more evidence that OMI is unable to retrieve NO_2 beneath thick clouds.



a.) Moles/Flash = -39.9 Limit = 2ppb

b.) Moles/Flash = 352.1 Limit = 2ppb



c.) Moles/Flash = -748.5 Limit = 2ppb

d.) Moles/Flash = -441.9 Limit = 2ppb

Figure 5: Total flashes with the sum of the total flashes above the plot, and LNO_x in kmoles with the sum of the total LNO_x in moles above the plot for a.) July 2nd, 2011, b.) July 3rd, 2011, c.) July 16th, 2011, d.) July 29th, 2011.

4.1.3 Conclusions

From our initial approach, we have determined that separate approaches are needed over deep convection and over clear regions. When viewing clear skies downwind of storms, subtracting a tropospheric background is necessary because OMI is observing the total column, from the top of the atmosphere to the surface. In instances of active convection, OMI cannot see the Earth's surface through the clouds, so subtracting a full tropospheric background is not appropriate, and will produce negative LNO_x values.

4.2 Active Convection Analysis – June 11th DC3 case

To explore the CRF influence on the column LNO_x, we analyzed one day from the Deep Convective Clouds and Chemistry (DC3) campaign. The DC3 experiment was a joint NSF/NASA campaign to understand the role of thunderstorms in upper tropospheric chemistry. Further discussion of the DC3 field campaign can be found in its Scientific Program Overview (*Barth et al., 2010*).

We chose to use DC3 days because aircraft in situ measurements are also available, which may aid in determining how our tropospheric background removal should be treated. The day used in this CRF threshold analysis is June 11th, 2012, on which measurements were taken during a storm event. To further aid with our CRF threshold analysis, we increased the vertical column LNO_x resolution from 2° x 2.5° to 1° x 1° latitude/longitude to provide more detailed spatial information.

To examine the effects of clouds on the OMI NO₂ retrievals, we applied four CRF thresholds, plotted in Figure 6. In plot a, no CRF threshold is applied (all pixels are used). The white region over western Missouri and Arkansas, and eastern Kansas and Oklahoma represents missing data due to the OMI row anomaly, and is clearly seen in all four plots.

In plot b, a CRF threshold of 70% is applied. Only pixels with an average CRF less than 70% are plotted. In plot c, a CRF threshold of 50% is applied, and in plot d a CRF threshold of 30% is applied. It is evident that as more stringent CRF thresholds are applied, and pixels with high average CRF values are removed from the analysis, so are useable OMI data. Since we are looking for NO₂ measurements over active convection, we can expect the average CRF for this case to be high.

In Figure 7, the OMI CRF values are shown for the same region as in Figure 6. Some pixels (shown in red) have a CRF > 100%. This is indicative of exceptionally high clouds due to active convection. As presented in Figure 7, a CRF of 70% and greater covers the majority of the storm region. It is also important to note that pixels with a CRF of 90% (shown in green) or greater, and pixels with the highest average vertical LNO₂ are collocated. From Figures 6 and 7, we conclude that removal of cloudy pixels with average CRFs of 70% or greater removes LNO_x data over active convection. OMI detects significant NO₂ above this region (as shown in Figure 6 plot a), so using CRF to isolate pixels over active convection may be more indicative of LNO_x measurements. To ensure our analysis (discussed in section 4.3) is done with pixels over the most actively convective regions of the storm, we isolate pixels with CRFs > 70% and CRFs > 90%.

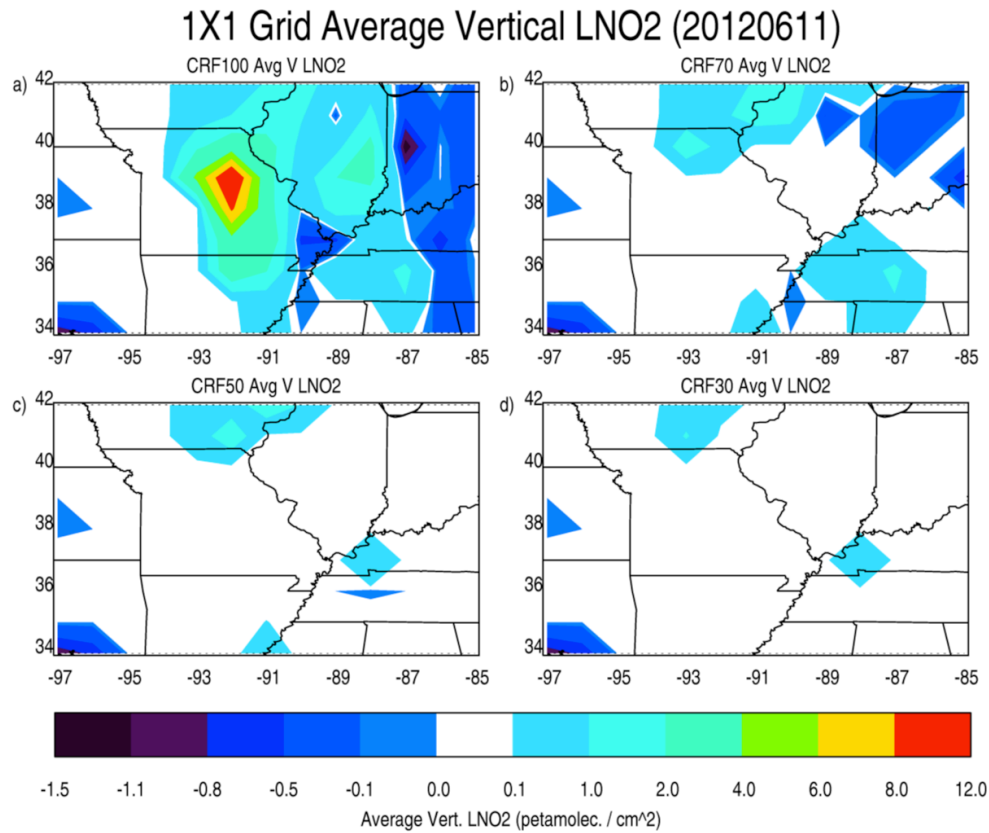


Figure 6: Plotted vertical LNO₂ for June 11th, 2012 on a 1° x 1° grid for a CRF threshold of 100% (all OMI pixels used), b CRF threshold of 70%, c CRF threshold of 50%, d CRF threshold of 30%

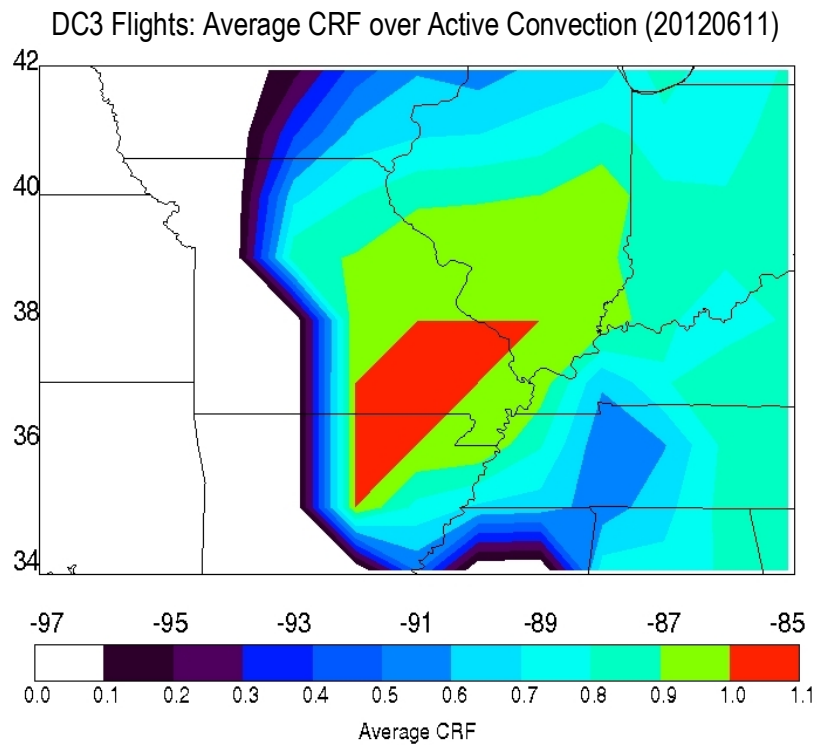


Figure 7: Average CRF on a 1° x 1° grid for the storm on June 11th, 2012. Note CRF values are above 1.0 or 100% (exceptionally high clouds).

4.3 Analysis with Active Convection over the Gulf of Mexico

For this analysis, we isolate all pixels with CRFs > 70%, and CRFs > 90%. The need for tropospheric background removal is negated with this method of OMI pixel isolation. To ensure storm events are detected, larger WWLLN flash thresholds of 100, 300, 500, and 1000 are applied. We continued to use a 6-hour time period prior to OMI overpass when accumulating WWLLN flash totals, but also conducted an analysis with a 3-hour time period prior to OMI overpass. These changes help isolate recent, strong storm events, likely to produce the LNO_x that OMI measures at the overpass time.

4.3.1 August 2008

Application of the adjustments to the algorithm and CRF criteria, along with lightning flash thresholds resolved many of the issues from the initial analysis. All figures in this section are for analysis executed with pixels that have a CRF > 70%.

In Figure 8, the daily moles per flash are plotted along with the total moles of LNO_x and total flashes for each day using flashes from the 6 hours prior to OMI overpass. In this figure, the total moles of LNO_x (blue) are scaled to correspond with the LNO_x moles per flash (black) values. This requires dividing the total moles by 10,000. The total flashes (red) are plotted using the axis to the right. All moles per flash values are positive, and range from about 20 to 400 moles per flash. In Figure 9, the August 2008 monthly averaged moles of LNO_x, WWLLN flashes, and LNO_x moles per flash are shown. Peaks in the monthly averaged lightning and LNO_x are collocated, a significant improvement from our initial analysis. A monthly average value of 236 LNO_x moles per flash is within the range of literature values (refer to Table 1).

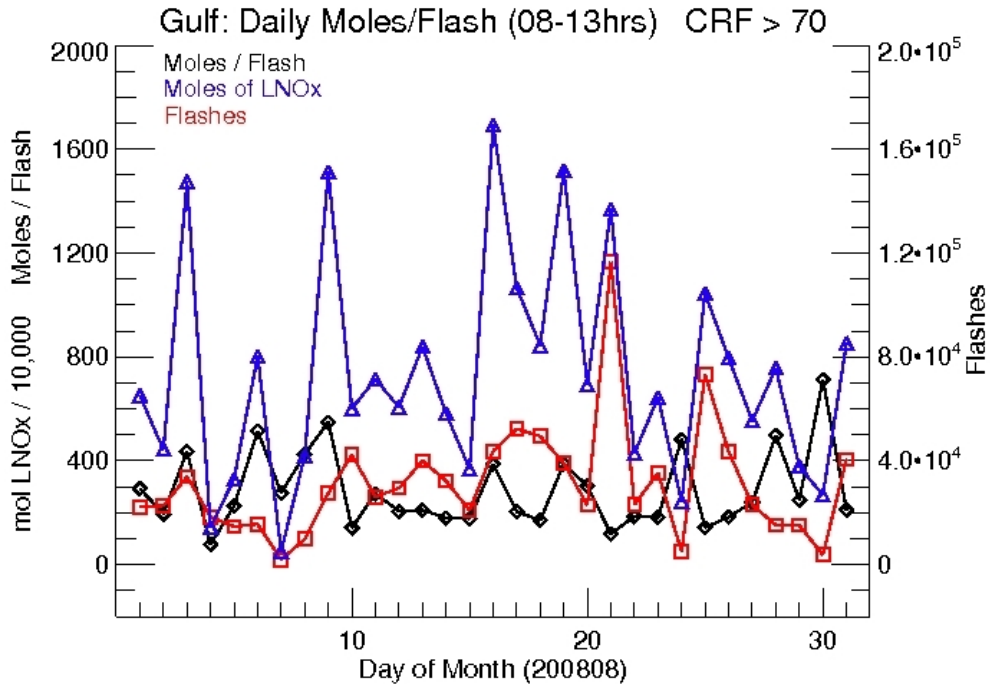


Figure 8: The blue line with triangle vertices represents moles of LNO_x/10,000; the red line with square vertices represents WWLLN flashes; and the solid line with diamond vertices represents moles per flash. This is plotted for the 6 hours prior to OMI overpass with flash threshold of 500 applied, and only pixels with a CRF > 70% are used.

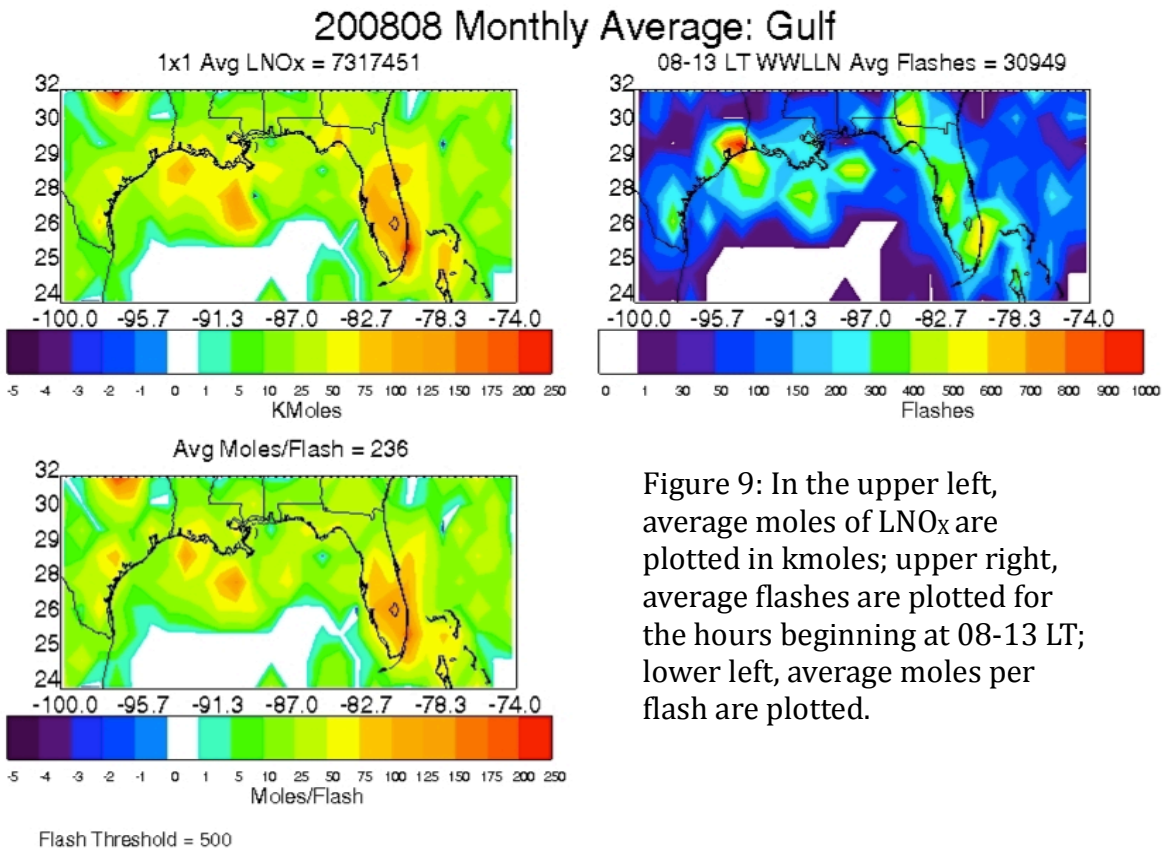


Figure 9: In the upper left, average moles of LNO_x are plotted in kmoles; upper right, average flashes are plotted for the hours beginning at 08-13 LT; lower left, average moles per flash are plotted.

Analysis for the shortened 3-hour time period prior to OMI overpass was also conducted. In Figure 10, the daily total moles of LNO_x (blue), total WWLLN flashes (red), and LNO_x moles per flash (black) are plotted. Compared to Figure 8, the moles per flash values have increased in Figure 10. This is an expected result because the time span prior to OMI overpass for determining the total flash count is smaller; so fewer flashes are attributed to the OMI observed LNO_x resulting in higher moles per flash values. It is worth noting that the number of grid boxes used to determine NO production per flash decreases when the flash accumulation period is decreased from 6 to 3 hours. Specifically, grid boxes that only experienced flashes between 08 and 11 LT are not included. Figure 11 shows the plotted monthly averaged total LNO_x, total WWLLN flashes for the 3-hour time period, and the average moles of LNO_x per flash. Adjusting to the 3-hours prior to OMI overpass has resulted in ~ 50% decrease in the total flashes, but only ~30% decrease in the total moles of LNO_x, resulting in an increased monthly averaged value of 330 moles of LNO_x per flash. This same analysis was also completed using pixels with CRFs > 90%, and for flash thresholds of 100, 300, and 1000. Figures for these analyses are not shown but the monthly averaged moles of LNO_x per flash values can be found in Table 2 (section 5).

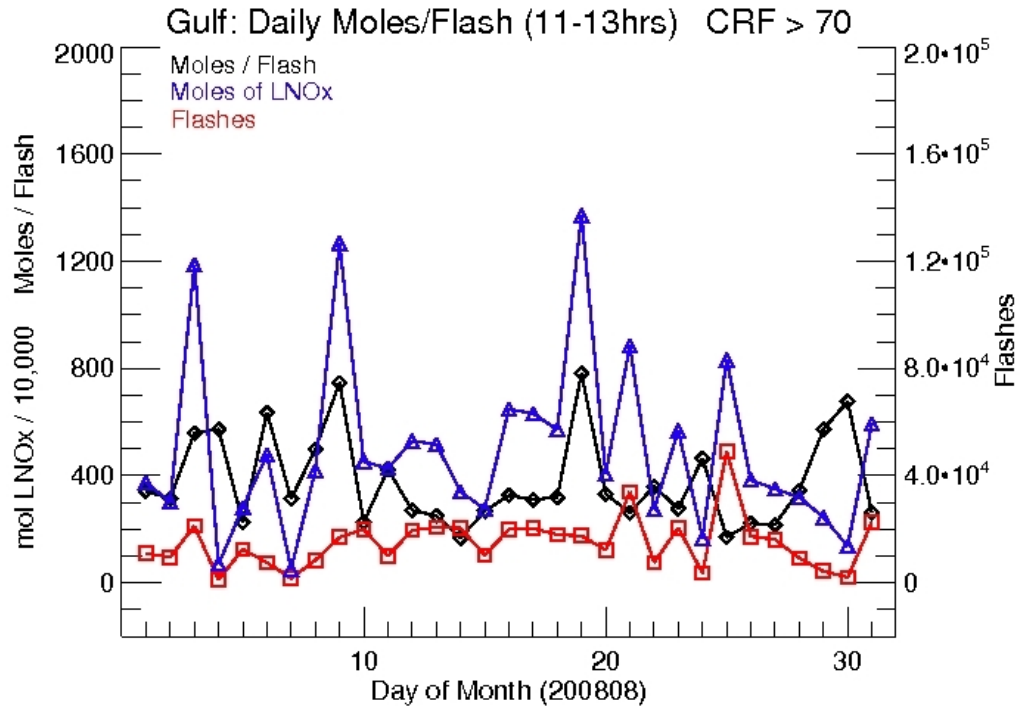


Figure 10: The blue line with triangle vertices represents moles of LNO_x/10,000; the red line with square vertices represents WWLLN flashes; and the solid line with diamond vertices represents moles per flash. This is plotted for the 3 hours prior to OMI overpass with flash threshold of 500 applied, and only pixels with a CRF > 70% are used.

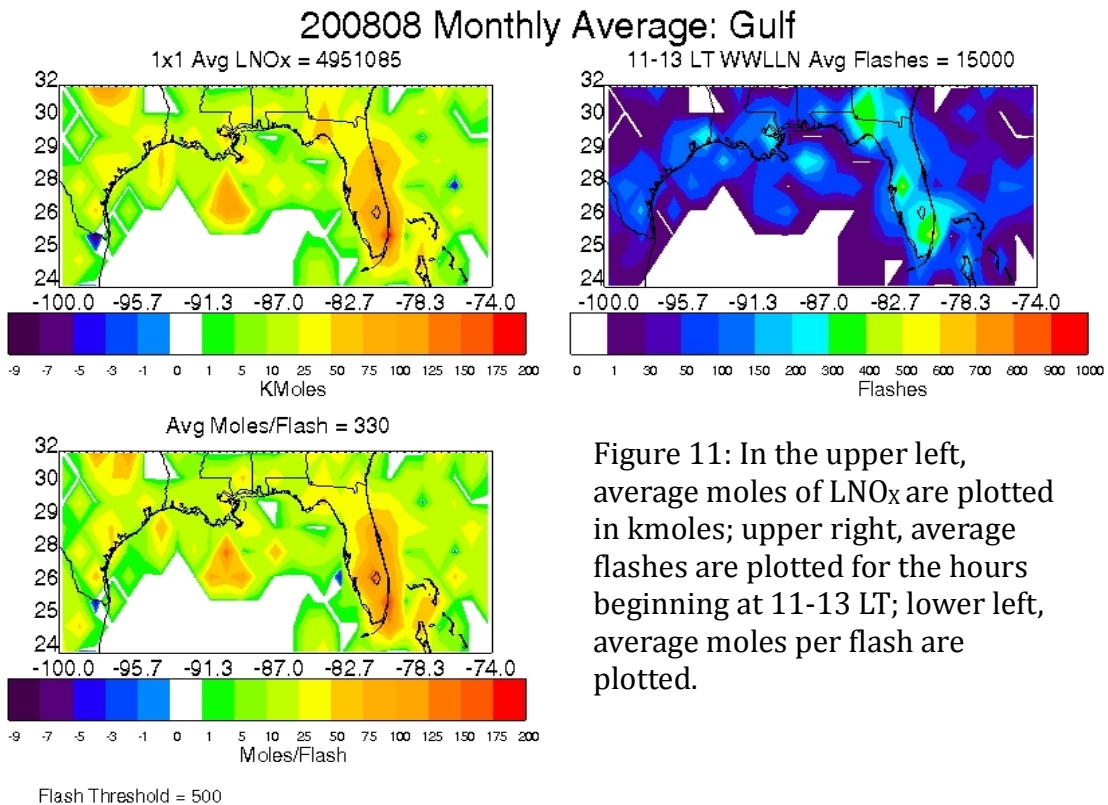


Figure 11: In the upper left, average moles of LNO_x are plotted in kmoles; upper right, average flashes are plotted for the hours beginning at 11-13 LT; lower left, average moles per flash are plotted.

4.3.2 July 2011

The same analysis as outlined in section 4.3.1 was completed for July 2011. Results from the analysis using pixels with a CRF > 90% are discussed for July 2011, but a similar analysis using pixels with a CRF > 70% was also executed (figures not shown). Due to the OMI row anomaly, analysis during July 2011 requires many days to be removed from the monthly average. The line plot (Figure 12) shows daily moles of LNO_x (blue), WWLLN flashes (red), and LNO_x moles per flash (black). The gaps in the data are indicative of days where the flash threshold was not met, no flashes were detected by WWLLN, or the OMI row anomaly affected too much of the Gulf of Mexico region for analysis to proceed. In terms of moles per flash, notice the two outlier days: the 8th and the 28th. Examination of the daily flashes reveals that for the 8th, flash counts for grid cells involved in the analysis are just above the flash threshold (500), causing the LNO_x moles per flash value to be quite high. For the 28th, the lightning flashes coincide with negative LNO_x values. The sources of the negative LNO_x values are unknown, further analysis is needed.

In Figure 13, the monthly average of moles of LNO_x, WWLLN flashes, and LNO_x moles per flash for pixels with CRFs > 90% reveal a similar result to those shown previously for August 2008. We found a monthly mean value of 293 moles of LNO_x per flash. There are peaks in lightning collocated with peaks in moles of LNO_x, however, a peak in LNO_x over the Gulf coast of Mississippi does not correspond to a significant peak in lightning. Further analysis is needed to determine the source of this monthly average LNO_x peak.

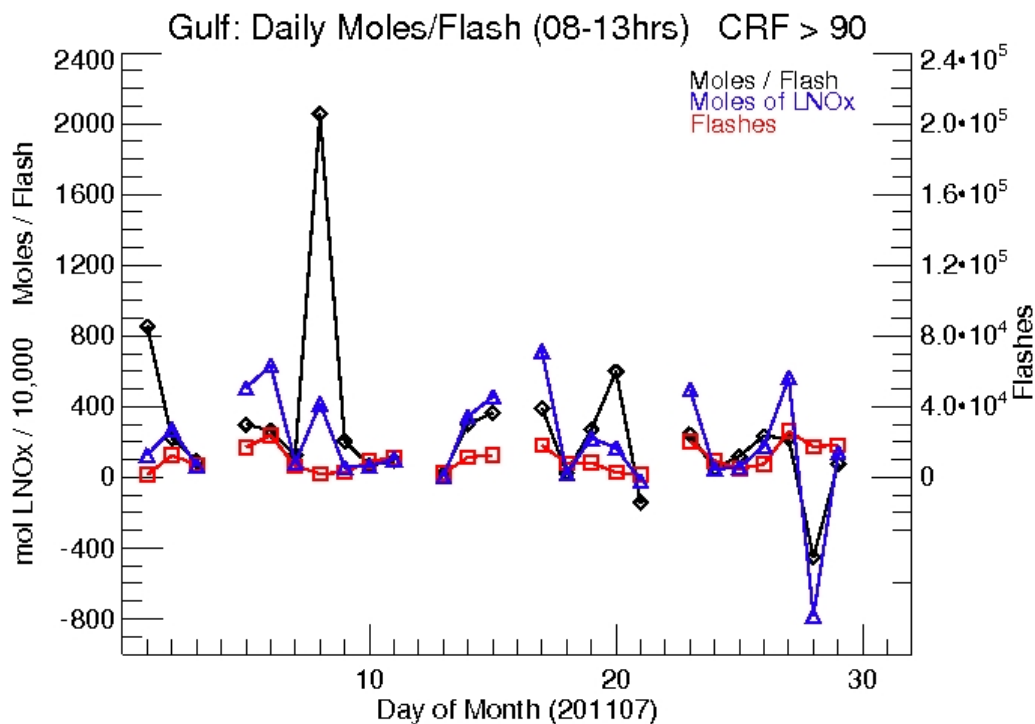


Figure 12: The blue line with triangle vertices represents moles of LNO_x/10,000; the red line with square vertices represents WWLLN flashes; and the solid line with diamond vertices represents moles per flash. This is plotted for the 6 hours prior to OMI overpass with a flash threshold of 500 applied, and only pixels with CRF > 90% are used.

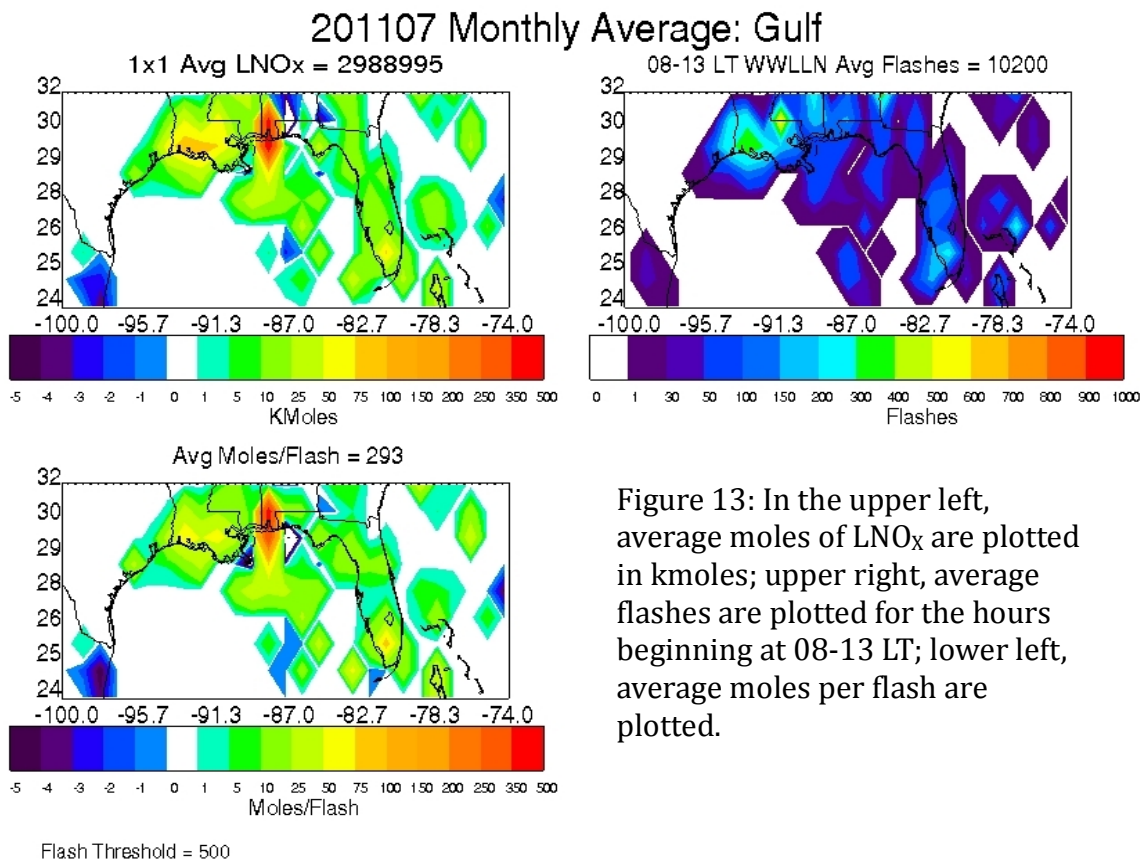


Figure 13: In the upper left, average moles of LNO_x are plotted in kmoles; upper right, average flashes are plotted for the hours beginning at 08-13 LT; lower left, average moles per flash are plotted.

In Figure 14, the daily total moles of LNO_x (blue), total WWLLN flashes (red), and moles per flash (black) values are shown as a line plot for the 3 hours prior to OMI overpass. Here we see many days with missing data, or data that do not meet the CRF and flash threshold (500) criteria. On July 8th, there is a significant jump in the moles per flash value because the total flashes are just above the flash threshold.

Figure 15 shows the monthly average moles of LNO_x, WWLLN flashes, and LNO_x moles per flash for the 3 hours prior to OMI overpass. As in the August 2008 analysis using pixels with a CRF > 70%, the total flashes and total moles of LNO_x values decrease when the time period is decreased from 6 hours to 3 hours. The total flashes decrease by ~40% while the total moles of LNO_x decrease by only ~20%. This results in a larger average moles per flash value of 372. Using pixels with CRFs > 90% removes grid boxes with lower kmoles of LNO_x from the analysis. These are grid boxes that are farther from convective cores, resulting in a higher mean moles per flash value for the region.

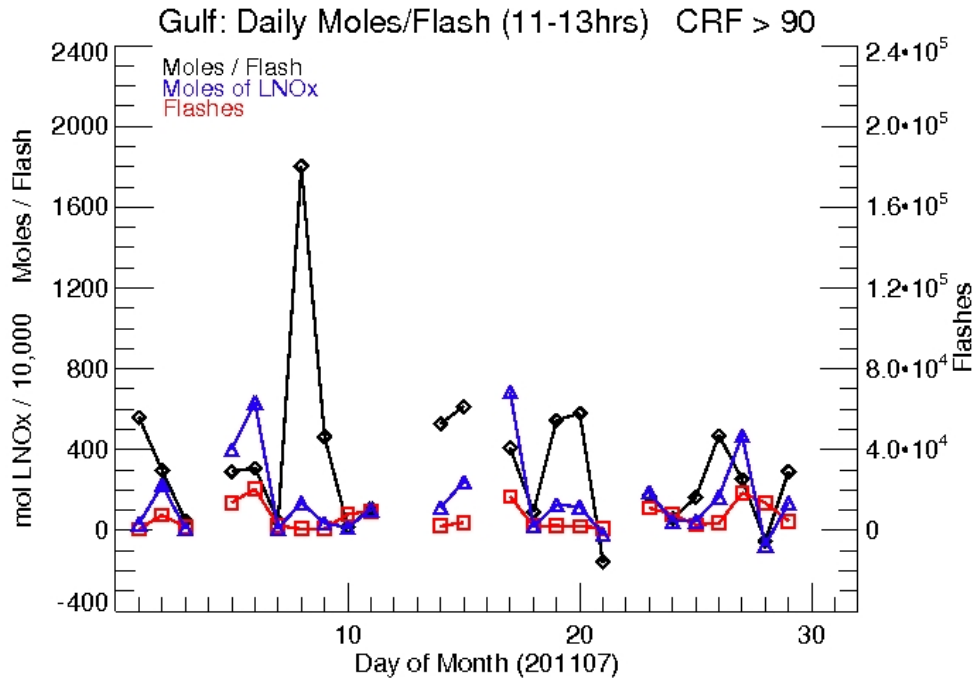


Figure 14: The blue line with triangle vertices represents moles of LNO_x/10,000; the red line with square vertices represents WWLLN flashes; and the solid line with diamond vertices represents moles per flash. This is plotted for the 3 hours prior to OMI overpass with a flash threshold of 500 applied, and only pixels with CRF > 90% are used.

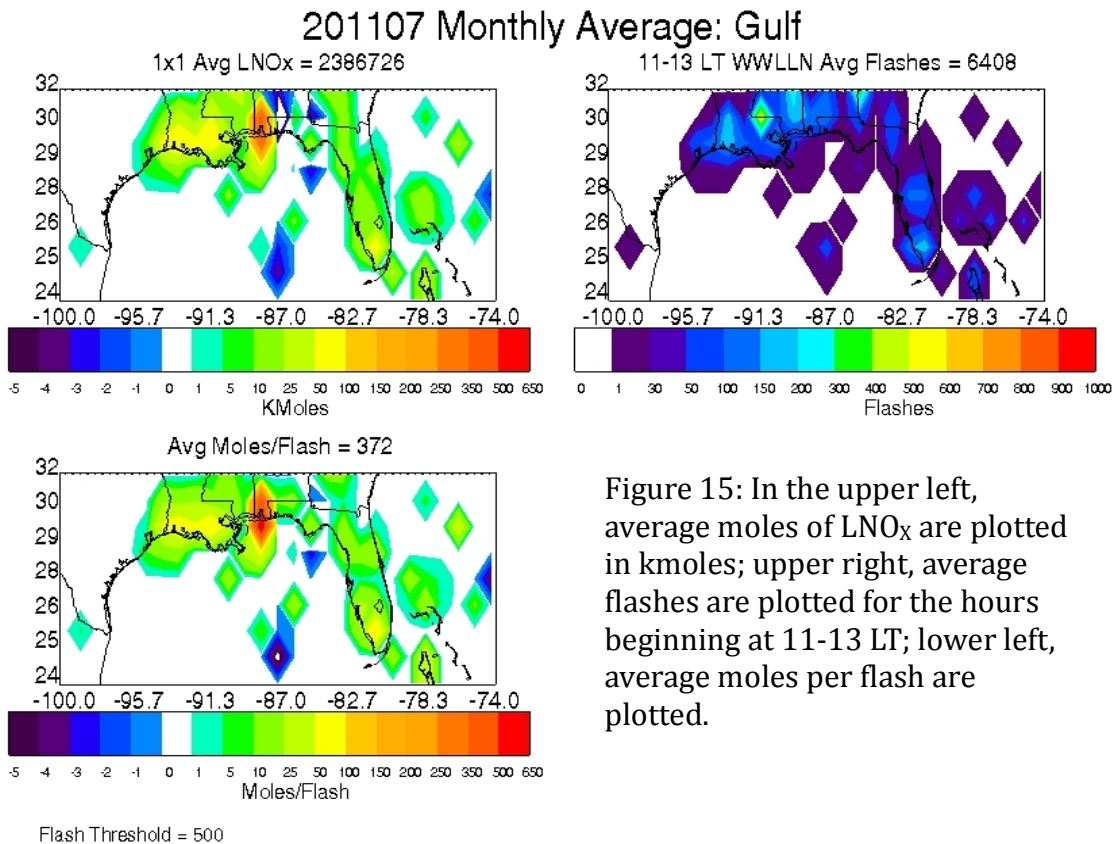


Figure 15: In the upper left, average moles of LNO_x are plotted in kmoles; upper right, average flashes are plotted for the hours beginning at 11-13 LT; lower left, average moles per flash are plotted.

5. Discussion and Conclusions

The results for all flash thresholds, for both 6 hour and 3 hour time periods, and for both CRF > 70% and CRF > 90% criteria are found in Table 2.

Table 2: All monthly averaged moles of LNO_x per flash results from CRF threshold analyses.

Month	Flash Threshold	Moles/Flash CRF > 90 08-13 hours	Moles/Flash CRF > 70 08-13 hours	Moles/Flash CRF > 90 11-13 hours	Moles/Flash CRF > 70 11-13 hours
August 2008	100	324	387	468	557
	300	250	278	350	400
	500	211	236	308	330
	1000	151	168	239	236
July 2011	100	624	498	680	587
	300	356	323	445	412
	500	293	268	372	329
	1000	216	206	165	203

For both months and both CRF criteria, the largest change in the LNO_x moles per flash values is seen when adjusting the flash threshold from 100 to 300. This means a significant amount of LNO_x is detected in grid boxes with flash totals under 300. A possible explanation for this is that LNO_x is moved into the grid box from a neighboring grid box, increasing the LNO_x attributed to the flashes. Further examination is necessary to determine the effects of transport on these calculations. When increasing the flash threshold from 300 to 500, the smallest change in moles per flash values is detected. Approximately 80% (July 2011) to 85% (August 2008) of the grid boxes with lightning have a total of 500 or more flashes. When transitioning the flash threshold from 500 to 1000, a large change in the moles per flash value is detected. This indicates that grid boxes with flashes totaling between 500 and 1000 have large LNO_x values. Eliminating these grid boxes may be removing data that should be included in the analysis. We therefore determine that a flash threshold of 500 is best for calculating the monthly average moles of LNO_x per flash values in the Gulf of Mexico region.

When comparing the CRF criteria, the moles per flash values using pixels with CRFs > 70% in August 2008, are almost always slightly higher than the values generated using pixels with CRFs > 90%. This means that the bulk of the pixels (~90%) used in calculating the moles per flash values have CRFs > 90%. This indicates that the majority of the active convection during the month typically produces bright clouds. Filtering OMI pixels based on a CRF > 90% criterion in the analysis for August 2008 is good for isolating active convection regions. For July 2011, the majority of the moles per flash values were generated using pixels with CRFs > 70%. This means that the clouds were lower and less bright, so when pixels with CRFs > 70% but < 90% were filtered from the analysis, we removed pixels and grid boxes with a significant portion of the LNO_x and flashes used in the moles per flash calculation. Since July 2011 relies upon using pixels with CRFs > 70%, and August 2008 values increase ~10% when using pixels with CRFs > 70%, we determine that using pixels with CRFs > 70% are best for calculating the moles of LNO_x per flash for the region.

From Table 2, we see that the moles per flash values are almost always larger for the 3 hours prior to OMI overpass than the 6 hours, regardless of the CRF criteria. For August 2008, ~30% and for July 2011, ~ 20% of the monthly average 6 hour moles per flash value comes from flashes that occurred between 08-11 LT. This means that ~ 70% and ~80% (2008 and 2011 respectively) of the moles per flash values come from flashes generated within the 3 hours prior to OMI overpass. We determine that totaling flashes in the 3 hours prior to OMI overpass is best for calculating the moles per flash values and decreases the probability of LNO_x being transported out of the grid box before the OMI overpass.

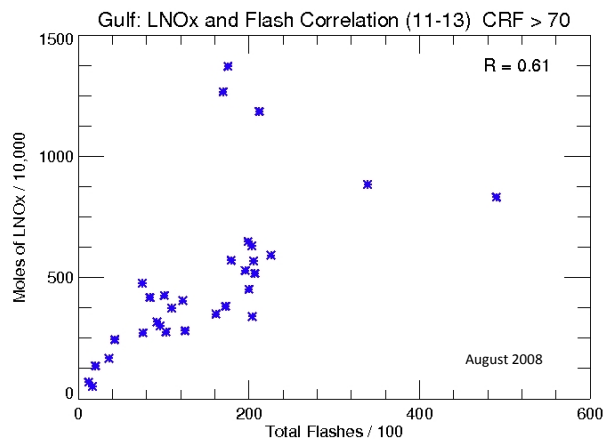


Figure 16: A correlation between the total flashes and total moles of LNO_x for each day in August 2008. The values used are for the flashes meeting the 500 flash threshold within the 3 hours prior to OMI overpass, and come from pixels with a CRF > 70%.

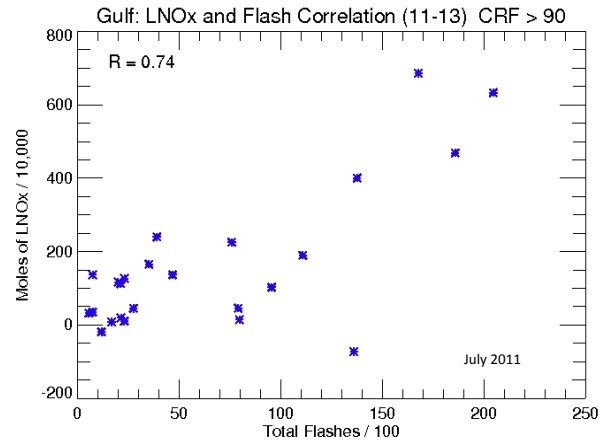


Figure 17: A correlation between the total flashes and total moles of LNO_x for each day in July 2011. The values used are for the flashes meeting the 500 flash threshold within the 3 hours prior to OMI overpass, and come from pixels with a CRF > 90%.

In both Figure 16 and 17, we see a positive correlation between the moles of LNO_x and the WWLLN flashes. For August 2008 (Figure 16) we find $R=0.61$ when analysis is done for the 3 hours prior to OMI overpass with a 500 flash threshold and uses pixels with a $CRF > 70\%$. This analysis includes all 31 days in the month. The R-value is lower than expected due to a few days used in the analysis. High LNO_x values corresponding to lower flash totals could mean LNO_x is being transported into the grid box. If these days are removed from the analysis, the remaining days have an R-value of 0.88. Further examination of these days is needed to justify removal from the analysis.

For July 2011 (Figure 17), we find $R=0.74$ when analysis is executed using a 500 flash threshold for the 3 hours prior to OMI overpass and pixels with CRFs > 90%. Note the different scales for the two plots; July 2011 has about half the LNO_x and half the flashes as August 2008. It is also important to note that 7 days are removed from the July 2011 analysis because they do not meet the various criteria. Further analysis is needed for the days when LNO_x values are negative.

Our method for separating the LNO_x signal from the total OMI measured NO₂ column may not be applicable for urban areas or locations affected by pollution from biomass burning. This method assumes that the CRF threshold removes the vast majority of any lower tropospheric NO₂ contributions, and thus attributes the total tropospheric portion of the measured NO₂ above the clouds to lightning. The values found in Table 2 for both CRF thresholds, and all flash thresholds fall within current literature estimates. The NO moles per flash estimates vary from 680 to 150, but most (18 of the 32 values shown) fall within the 200-350 moles per flash range. Our best estimate is ~330 moles of LNO_x per flash for the Gulf of Mexico region, as this is the value obtained for CRF>70%, with using flashes in the 3 hours prior to OMI overpass, and with a threshold of 500 flashes for both months analyzed.

The region lies on the border between the tropics and mid-latitudes, and we find most of our estimates coincide with the literature values found for the tropics, as detailed in Table 1. The analysis for August 2008 is best and most complete due to the OMI data availability and reliability. We believe the 3 hours prior to OMI overpass and values with flash thresholds of 500 and 1000 are most indicative of LNO_x produced from active convection. A time frame shorter than 6 hours ensures the LNO_x is not transported out of the area of analysis, and higher flash thresholds ensure only grid boxes with significant storm activity are included in the analysis.

Analyses of other summer months and other years within the Gulf of Mexico region are necessary to determine if the NO moles per flash values shown in this study are consistent over a longer period. Similarly, analyses in other high lightning activity regions like Central Africa, Central America, and Indonesia are necessary to further examine this method.

A global application of the LNO_x algorithm will need further adjustments to account for human activity (anthropogenic emissions), continental and maritime variation, and to ensure long-range transport in the free troposphere is attributed to the appropriate upwind lightning flashes. Individual storm case studies will help to improve our analysis methods, and aid in the development of an algorithm for global application. Further analysis over clear sky (CRF < 30%) is necessary to capture the long-range transport of LNO_x. To accurately extract the LNO_x signal in clear skies, introduction of a background estimate is necessary. Correct implementation of this lower tropospheric background will require further analysis.

Acknowledgements

This research was funded under the NASA Master Grant NNX12AD03A under the cooperative agreement between the Earth System Science Interdisciplinary Center (ESSIC) at the University of Maryland and NASA Goddard.

I would like to thank my advisors Dr. Kenneth Pickering and Dr. Dale Allen for their support, guidance, expertise and patience throughout the course of my research.

6. References

- Allen, D. J. and K. E. Pickering (2002), Evaluation of lightning flash rate parameterizations for use in a global chemical transport model, *Journal of Geophysical Research*, 107(D23), 4711, doi:10.1029/2002JD002066.
- Allen, D. J., K. E. Pickering, B. Duncan, and M. Damon (2010), Impact of lightning NO emissions on North American photochemistry as determined using the Global Modeling Initiative (GMI) model, *Journal of Geophysical Research*, 115, D22301, doi:10.1029/2010JD014062.
- Allen, D. J., A. Ring, K. Pickering, A. Nag, R. Holle, and R. Holzworth (2014), Analysis of Ground Network Lightning Data Relative to OTD/LIS to Derive Flash Rates for Use in Determining Lightning NO_x Production from Satellite Observation, ILDC/ILMC 2014, Tucson, AZ.
- Barth, M.C., C. A. Cantrell, W. Brune, S. Rutledge, O. R. Cooper, J. H. Crawford, A. Fried, A. Heymsfield, P. R. Krehbiel, D. MacGorman, L. Pan, W. Petersen, K. E. Pickering, J. Stith, and A. Weinheimer (2010), Scientific Program Overview (SPO) for a Deep Convective Clouds and Chemistry (DC3) Field Campaign, *Submitted to the National Science Foundation*, Jan 2009, revised Aug 2010.
- Beirle, S., N. Spichtinger, A. Stohl, K. L. Cummins, T. Turner, D. Boccippio, O. R. Cooper, M. Wenig, M. Grzegorski, U. Platt, and T. Wagner (2006), Estimating the NO_x produced by lightning from GOME and NLDN data: a case study in the Gulf of Mexico, *Atmospheric Chemistry and Physics*, 6, 1075-1089.
- Beirle, S., M. Salzmann, M. G. Lawrence, and T. Wagner (2009), Sensitivity of satellite observations for freshly produced lightning NO_x, *Atmospheric Chemistry and Physics*, 9, 1077-1094.
- Beirle, S., H. Huntrieser, and T. Wagner (2010), Direct satellite observation of lightning-produced NO_x, *Atmospheric Chemistry and Physics*, 10, 10965-10986, doi:10.5194/acp-10-10965-2010.
- Boccippio, D. J., W. J. Koshak, and R. J. Blakeslee (2002), Performance assessment of the Optical Transient Detector and Lightning Imaging Sensor. Part I: Predicted Diurnal Variability, *Journal of Atmospheric and Oceanic Technology*, 19, 1318-1332.
- Boersma, K. F., H. J. Eskes, R. J. Dirksen, R. J. van der A, J. P. Veefkind, P. Stammes, V. Huijnen, Q. J. Kleipool, M. Sneep, J. Claas, J. Leitao, A. Richter, Y. Zhou, and D. Brunner (2011), An improved tropospheric NO₂ column retrieval algorithm for the Ozone Monitoring Instrument, *Atmospheric Measurement Techniques Discussion*, 4, 2329-2388, doi:10.5194/amtd-4-2329-2011.

- Bucsela, E. J., K. E. Pickering, T. J. Huntemann, R. C. Cohen, A. Perring, J. F. Gleason, R. J. Blakeslee, R. I. Albrecht, R. H. Holzworth, J. P. Cipriani, D. Vargas-Navarro, I. Mora-Segura, A. Pacheco-Hernández, and S. Laporte-Molina (2010), Lightning-generated NO_x seen by the Ozone Monitoring Instrument during NASA's Tropical Composition, Cloud and Climate Coupling Experiment (TC⁴), *Journal of Geophysical Research*, 115, D00J10, doi:10.1029/2009JD013118.
- Bucsela, E. J., N. A. Krotkov, E. A. Celarier, L. N. Lamsal, E. H. Swartz, P. K. Bhartia, K. F. Boersma, J. P. Veefkind, J. F. Gleason, and K. E. Pickering (2013), A new stratospheric and tropospheric NO₂ retrieval algorithm for nadir-viewing satellite instruments: applications to OMI, *Atmospheric Measurement Techniques*, 6, 2607-2626, doi:10.5194/amt-6-2607-2013.
- Cecil, D. J., D. E. Buechler, and R. J. Blakeslee (2012), Gridded Lightning Climatology from TRMM-LIS and OTD: Dataset Description, *Atmospheric Research*, 2012, doi:10.1016/j.atmosres.2012.06.028.
- Christian, H. J., R. J. Blakeslee, S. J. Goodman, D. A. Mach, M. F. Stewart, D. E. Buechler, W. J. Koshak, J. M. Hall, W. L. Boeck, K. T. Driscoll, and D. J. Boccippio (1999), The Lightning Imaging Sensor, *NASA Conference Publication*, 746-749, http://thunder.msfc.nasa.gov/bookshelf/pubs/LIS_ICAE99_Print.pdf.
- Christian, H. J., R. J. Blakeslee, D. J. Boccippio, W. L. Boeck, D. E. Buechler, K. T. Driscoll, S. J. Goodman, J. M. Hall, W. J. Koshak, D. M. Mach, and M. F. Stewart (2003), Global frequency and distribution of lightning as observed from space by the Optical Transient Detector, *Journal of Geophysical Research*, 108(D1), 4005, doi:10.1029/2002JD002347.
- Cummings, K. A., T. L. Huntemann, K. E. Pickering, M. C. Barth, W. C. Skamarock, H. Holler, H. -D. Betz, A. Volz-Thomas, and H. Schlager (2013), Cloud-resolving chemistry simulation of a Hector thunderstorm, *Atmospheric Chemistry and Physics*, 13, 2737-2777, doi:10.5194/acp-13-2757-2013.
- DeCaria, A. J., K. E. Pickering, G. L. Stenchikov, J. R. Scala, J. L. Stith, J. E. Dye, B. A. Ridley, and P. Laroche (2000), A cloud-scale model study of lightning-generated NO_x in an individual thunderstorm during STERAO-A, *Journal of Geophysical Research*, 105(D9), 11,601-11,616.
- DeCaria, A. J., K. E. Pickering, G. L. Stenchikov, and L. E. Ott (2005), Lightning-generated NO_x and its impact on tropospheric ozone production: A three-dimensional modeling study of a Stratosphere-Troposphere Experiment: Radiation, Aerosols, and Ozone (STERAO-A) thunderstorm, *Journal of Geophysical Research*, 110, D14303, doi:10.1029/2004JD005556.
- Dowden, R. J., J. B. Brundell, and C. J. Rodger (2002), VLF lightning location by time of group arrival (TOGA) at multiple sites, *Journal of Atmospheric and Solar-Terrestrial Physics*, 64, 817-830.

- Duncan, B. N., S. E. Strahan, Y. Yoshida, S. D. Steenrod, and N. Livesey (2007), Model study of the cross-tropopause transport of biomass burning pollution, *Atmospheric Chemistry and Physics*, 7, 3713-3736.
- Gallardo, L., and V. Cooray (1996), Could cloud-to-cloud discharges be as effective as cloud-to-ground discharges in producing NO_x?, *Tellus*, 4b, 641-651.
- Hauglustaine, D., L. Emmons, M. Newchurch, G. Brasseur, T. Takao, K. Matsubara, J. Johnson, B. Ridley, J. Stith, and J. Dye (2001), *Journal of Atmospheric Chemistry*, 38, 277-294.
- Huntrieser, H., C. Feigl, H. Schlager, F. Schöder, C. Gerbig, P. van Velthoven, F. Flatøy, C. Théry, A. Petzold, H. Höller, and U. Schumann (2002), Airborne measurements of NO_x tracer species, and small particles during the European Lightning Nitrogen Oxides Experiment, *Journal of Geophysical Research*, 107, D11, doi:10.1029/2000JD000209.
- Huntrieser, H., U. Schumann, H. Schlager, H. Höller, A. Giez, H.-D. Betz, D. Brunner, C. Forster, O. Pinto Jr., and R. Calheiros (2008), Lightning activity in Brazilian thunderstorms during TROCCINOX: implications for NO_x production, *Atmospheric Chemistry and Physics*, 8, 921-953.
- Huntrieser, H., H. Schlager, M. Lichtenstern, A. Roiger, P. Stock, A. Minikin, H. Höller, K. Schmidt, H.-D. Betz, G. Allen, S. Viciani, A. Ulanovsky, F. Ravengnani, and D. Brunner (2009), NO_x production by lightning in Hector: first airborne measurements during SCOUT-O3/ACTIVE, *Atmospheric Chemistry and Physics*, 9, 8377-8412.
- Huntrieser, H., H. Schlager, M. Lichtenstern, P. Stock, T. Hamburger, H. Höller, K. Schmidt, H.-D. Betz, A. Ulanovsky, and F. Ravengnani (2011), Mesoscale convective systems observed during AMMA and their impact on the NO_x and O₃ budget over West Africa, *Atmospheric Chemistry and Physics*, 11, 2503-2536.
- Hutchins, M. L., R. H. Holzworth, K. S. Virts, J. M. Wallace, and S. Heckman (2013), Radiated VLF energy differences of land and oceanic lightning, *Geophysical Research Letters*, 40, 2390-2394, doi:10.1002/grl.50406.
- IPCC, 2013: Climate Change 2013: The Physical Science Basis. Contribution of Working Group I to the Fifth Assessment Report of the Intergovernmental Panel on Climate Change [Stocker, T. F., D. Qin, G. -K. Plattner, M. Tignor, S. K. Allen, J. Boschung, A. Nauels, Y. Xia, V. Bex, and P. M. Midgley (eds.)]. Cambridge University Press, Cambridge, United Kingdom and New York, NY, USA, 1535 pp.
- Jaeglé, L., D. J. Jacob, Y. Wang, A. J. Weinheimer, B. A. Ridley, T. L. Campos, G. W. Sachse, and D. E. Hagen (1998), Sources and chemistry of NO_x in the upper troposphere over the United States, *Geophysical Research Letters*, 25, No. 10, 1705-1708.

- Koshak, W., H. Peterson, A. Biazar, M. Khan, and L. Wang (2014), The NASA Lightning Nitrogen Oxides Model (LNOM): Application to air quality modeling, *Atmospheric Research*, <http://dx.doi.org/10.1016/j.atmosres.2012.12.015>.
- Labrador, L. J., R. von Kuhlmann, and M. G. Lawrence (2005), The effects of lightning-produced NO_x and its vertical distribution on atmospheric chemistry: sensitivity simulations with MATCH-MPIC, *Atmospheric Chemistry and Physics*, 5, 1815-1834.
- Lay, E. H., R. H. Holzworth, C. J. Rodger, J. N. Thomas, O. Pinto, and R. L. Dowden (2004), WWLL global lightning detection system: Regional validation study in Brazil, *Geophysical Research Letters*, 31, L03102, doi:10.1029/2003GL018882.
- Lay, E. H., C. J. Rodger, R. H. Holzworth, and R. L. Dowden (2005), Introduction to the World Wide Lightning Location Network (WWLLN), *Geophysical Research Abstracts*, 7, 02875, SRef-ID:1607-7962/gra/EGU05-A-02875.
- Levelt, P. F., G. H. J. van den Oord, M. R. Dobber, A. Mälkki, H. Visser, J. de Vries, P. Stammes, J. O. V. Lundell, and H. Saari (2006a), The Ozone Monitoring Instrument, *IEEE Transactions on Geoscience and Remote Sensing*, 44, No. 5, 1093-1101.
- Levelt, P. F., E. Hilsenrath, G. W. Leppelmeier, G. H. J. van den Oord, P. K. Bhartia, J. Tamminen, J. F. de Haan, J. P. Veefkind (2006b), Science Objectives of the Ozone Monitoring Instrument, *IEEE Transactions on Geoscience and Remote Sensing*, 44, No. 5, 1199-1208.
- Mach, D. M., H. J. Christian, R. J. Blakeslee, D. J. Boccippio, S. J. Goodman, and W. L. Boeck (2007), Performance assessment of the Optical Transient Detector and Lightning Imaging Sensor, *Journal of Geophysical Research*, 112, D09201, doi:10.1029/2006JD007787.
- Martin, R. V., B. Sauvage, I. Folkins, C. E. Sioris, C. Boone, P. Bernath, and J. Ziemke (2007), Space-based constraints on the production of nitric oxide by lightning, *Journal of Geophysical Research*, 112, D09309, doi:10.1029/2006JD007831.
- Ott, L. E., K. E. Pickering, G. L. Stenchikov, H. Huntrieser, and U. Schumann (2007), Effects of lightning NO_x production during the 21 July European Lightning Nitrogen Oxides Project storm studied with a three-dimensional cloud-scale chemical transport model, *Journal of Geophysical Research*, 112, D05307, doi:10.1029/2006JD007365.
- Ott, L. E., K. E. Pickering, G. L. Stenchikov, D. J. Allen, A. J. DeCaria, B. Ridley, R.-F. Lin, S. Lang, and W.-K. Tao (2010), Production of lightning NO_x and its vertical distribution calculated from three-dimensional cloud-scale chemical transport model simulations, *Journal of Geophysical Research*, 115, D04301, doi:10.1029/2009JD011880.

- Pickering, K. E., A. M. Thompson, W.-K. Tao, and T. L. Kucsera (1993), Upper tropospheric ozone production following mesoscale convection during STEP/EMEX, *Journal of Geophysical Research*, 98(D5), 8,737-8,749.
- Pickering, K. E., A. M. Thompson, Y. Wang, W.-K. Tao, D. P. McNamara, V. W. J. H. Kirchhoff, B. G. Heikes, G. W. Sachse, J. D. Bradshaw, G. L. Gregory, and D. R. Blake (1996), Convective transport of biomass burning emissions over Brazil during TRACE A, *Journal of Geophysical Research* 101(D19), 23,993-24,012.
- Pickering, K. E., Y. Wang, W.-K. Tao, C. Price, J.-F. Müller (1998), Vertical distributions of lightning NO_x for use in regional and global chemical transport models, *Journal of Geophysical Research*, 103(D23), 31,203-31,216.
- Pickering, K. E., D. J. Allen, A. Ring, E. Bucsela, A. Nag, and R. Holle (2014), Lightning NO_x Production per Flash based on OMI NO₂ Observations and Ground Network Lightning Data, ILDC/ILMC 2014, Tucson, AZ.
- Platt, U. and Stutz, J. (2006), Differential Optical Absorption Spectroscopy (DOAS), Principle and Applications, *Springer Verlag Heidelberg*, ISBN 3-340-21193-4.
- Price, C., J. Penner, and M. Prather (1997), NO_x from lightning 2. Constraints from the global atmospheric electric circuit, *Journal of Geophysical Research*, 102(D5), 5,943-5,951.
- Rienecker, M. M., M. J. Suarez, R. Todling, T. Bacmeister, L. Takacs, H.-C. Liu, W. Gu, M. Sienkiewicz, R. D. Koster, R. Gelaro, I. Stajner, and J. E. Nielsen (2008), the GEOS-f Data Assimilation System-Documentation of Versions 5.0.1, 5.1.0, and 5.2.0, *Technical Report Series on Global Modelin and data Assimilation*, NASA/TM-2008-104606, Vol. 27.
- Rodger, C. J., J. B. Brundell, R. L. Dowden, and N. R. Thomson (2004), Location accuracy of long distance VLF lightning location network, *Annals Geophysicae*, 22, 747–758.
- Rodger, C. J., J. B. Brundell, and R. L. Dowden (2005), Location accuracy of VLF World-Wide Lightning Location (WWLL) network: Post-algorithm upgrade, *Annals Geophysicae*, 23, 277–290.
- Rodger, C. J. J. B. Brundell, R. H. Holzworth, E. H. Lay (2009), Growing Detection Efficiency of the World Wide Lightning Location Network, *AIP Conference Proceedings*, 1118, doi:10.1063/1.3137706.
- Rudlosky, S. D. and D. T. Shea (2013), Evaluating WWLLN performance relative to TRMM/LIS, *Geophysical Research Letters*, 40, 1-5, doi:10.1002/grl.50428.
- Schumann, U. and H. Huntrieser (2007), The global lightning-induced nitrogen oxides source, *Atmospheric Chemistry and Physics*, 7, 3823-3907.

- Seinfeld, J. H. and S. N. Pandis (2006), Atmospheric Chemistry and Physics: From Air Pollution to Climate Change, *Wiley-Interscience*, ISBN: 978-0-471-72018-8.
- Tie, X., R. Zhang, G. Brasseur, and W. Lei (2002), Global NO_x production by lightning, *Journal of Atmospheric Chemistry*, 43, 61-74.
- van der Werf, G. R., J. T. Randerson, L. Giglio, G. J. Collatz, M. Mu, P. S. Kasibhatla, D. C. Morton, R. S. DeFries, Y. Jim, and T. T. van Leeuwen (2010), Global fire emissions and the contribution of deforestation, savanna, forest, agricultural, and peat fires (1997-2009), *Atmospheric Chemistry and Physics*, 10, 11,707-11,735.
- van Donkelaar, A., R. V. Martin, W. R. Leaitch, A. M. Macdonald, T. W. Walker, D. G. Streets, Q. Zhang, E. J. Dunlea, J. L. Jimenez, J. E. Dibb, L. G. Huey, R. Weber, and M. O. Andreae (2008), Analysis of aircraft and satellite measurements from the Intercontinental Chemical Transport Experiment (INTEX-B) to quantify long-range transport of East Asian sulfur to Canada, *Atmospheric Chemistry and Physics*, 8, 2999-3014.
- Virts, K. S., J. M. Wallace, M. L. Hutchins, and R. H. Holzworth (2013), Highlights of a new ground-based, hourly global lightning climatology, *Bulletin of the American Meteorological Society*, 94, 1381-1392.
- Wang, Y., A. W. DeSilva, G. C. Goldenbaum, and R. R. Dickerson (1998), Nitric oxide production by simulated lightning: Dependence on current, energy, and pressure, *Journal of Geophysical Research*, 103(D15), 19,149-19,159.
- Yevich, R. and J. A. Logan (2003), An assessment of biofuel use and burning of agricultural waste in the developing world, *Global Biogeochemical Cycles*, 17 (4), 1095, doi:10.1029/2002GB001952.
- Zeldovich, Y. B., P. Y. Sadovnikov, and D. A. Frank-Kamenetskii (1947), Oxidation of Nitrogen in Combustion, M. Shelef. Trans., *Academy of Sciences of USSR*, Institute of Chemical Physics, Moscow-Leningrad.
- Zhang, Q., D. G. Streets, G. R. Carmichael, K. B. He, H. Huo, A. Kannari, Z. Klimont, I. S. Park, S. Reddy, J. S. Fu, D. Chen, L. Duan, Y. Lei, L. T. Wang, and Z. L. Yao (2009), Asian emissions in 2006 for the NASA INTEX-B mission, *Atmospheric Chemistry and Physics*, 9, 5131-5153.
- Zhang, R., X. Tie, and D. W. Bond (2003), Impacts of anthropogenic and natural NO_x sources over the U.S. on tropospheric chemistry, *Proceedings of the National Academy of Sciences*, 100, No. 4, 1505-1509.
- Ziemke, J. R., S. Chandra, B. N. Duncan, L. Froidevaux, P. K. Bhartia, P. F. Levelt, and J. W. Waters (2006), Tropospheric ozone determined from Aura OMI and MLS: Evaluation of measurements and comparison with the Global Modeling Initiative's Chemical Transport Model, *Journal of Geophysical Research*, 111, D19303, doi:10.1029/2006JD007089.